Analyzing consequences to astrocytes in a mouse model of brain arteriovenous malformation

---

A Thesis

Presented to

The Honors Tutorial College

Ohio University

In Partial Fulfillment

of the Requirements for Graduation

from the Honors Tutorial College

with the degree of

Bachelor of Science in Neuroscience

By

Brittney M. Ward

April 2021

This thesis has been approved by

The Honors Tutorial College and the Department of Biological Sciences

_____

Dr. Corinne Nielsen

Assistant Professor, Biological Sciences

Thesis Advisor

_____

Dr. Janet Duerr

Director of Studies, Neuroscience

_____

Dr. Donal Skinner

Dean, Honors Tutorial College

Abstract

Arteriovenous malformation (AVM) is a disease where the typical connections between arteries and veins are abnormal and enlarged, so blood flows more directly from arteries to veins. These enlarged vessels have compromised integrity and are very susceptible to rupture. Though it only affects 0.01% of the population, AVM accounts for 2% of all strokes. AVM can also cause other issues such as aneurism, migraines, and seizures. Treatments for AVM are limited, in part because of a lack of understanding about how the disease occurs and progresses. This thesis uses a mouse model of AVM that manipulates an important developmental signaling pathway to produce AVM-like abnormal arteriovenous connections. Using such disease models, we can advance our understanding of AVM and of potential treatments for AVM.

Astrocytes are cells in the brain that contribute to tissue homeostasis and the blood-brain barrier. When the brain sustains damage or disease, astrocytes undergo changes to react and respond to the injury. These are known as reactive astrocytes. These astrocytes can respond in a myriad of ways. There is currently very little research on astrocytes in brain AVM. Astrocytes play such a vital role in brain homeostasis and repair processes that it would be very clinically relevant to understand how AVM affects them. In this thesis, I sought to determine whether astrocytes are reactive in the mouse model of AVM by testing hypertrophy and proliferation, two characteristics of reactive astrocytes. I also assessed levels of glial fibrillary acidic protein (GFAP) through measuring microscope image area, protein expression, and transcript expression in astrocytes. I also tested for changes in other transcripts that could provide evidence in support of astrocyte reactivity. Astrocyte hypertrophy and proliferation increased in the AVM mutant, as compared to controls, suggesting that astrocytes became reactive during AVM pathogenesis. Cortical and cerebellar tissue area with GFAP-positive astrocytes trended toward increased area;

however, this analysis needs higher sample size to be able to draw statistical and biological conclusions. Toward understanding molecular changes to AVM-mutant astrocytes, I isolated an enriched astrocyte population from early postnatal mouse brain. Using these isolated cells, I initiated experiments to assess select transcript levels from control and mutant samples. Preliminary data showed successful amplification of products from *Gfap*, *β-actin*, *Aldh1L1*, and *C3* transcripts. These experiments will accelerate our ability to determine gene expression changes in AVM mutant astrocytes, as compared to controls. The work described in this thesis represents a new avenue of brain AVM research in our lab and in the field, to understand consequences to astrocytes during brain AVM.

Table of Contents

INTRODUCTION **6**

Arteriovenous Malformation **6**

AVM in Humans **7**

Treatment/Management **9**

Notch Signaling **10**

AVM Mouse Model **13**

Neurovascular Unit **15**

Astrocytes **16**

Reactive Astrogliosis in Disease and Injury **18**

Astrocytes in Brain AVM and Hypothesis **20**

METHODS: **23**

Mice **23**

Genotyping **23**

Cre Responsive Genetic Labeling **25**

Immunostaining **26**

Proliferation Assay/EdU **27**

Western Blot **28**

Astrocyte Cell Isolation **29**

qPCR **30**

Analyses **32**

RESULTS **33**

Astrocyte projection diameter increased in cerebellum of P14 Rbpj$^{i\Delta EC}$ mutant mice 33

Number of GFAP and EdU double-positive cells increased in P14 Rbpj$^{i\Delta EC}$ cortex 35

GFAP positive area did not change in mutant cortex, cerebellum, and brain stem .37

Aldh1L1 protein expression did not change in Rbpj mutant 39

Transcript expression did not show significant change in enriched astrocyte cell population of Rbpj mutant 40

DISCUSSION: 42

FUTURE DIRECTIONS 50

CONCLUSION 51

ACKNOWLEDGEMENTS 52

WORKS CITED 54

INTRODUCTION

Arteriovenous Malformation

The circulatory system delivers nutrients and oxygen to all tissues within the body through blood circulating in vessels. Arteries are the vessels that carry oxygen-rich blood away from the heart and to the tissues of the body, and veins are the vessels that carry the blood back to the heart, once oxygen and carbon dioxide have been exchanged in tissues. Arteries and veins are connected by a network of thin vessels known as capillaries. Capillaries are where exchange of oxygen, carbon dioxide, and nutrients take place. Brain vasculature requires special reinforcement to ensure that pathogens and toxins from the blood do not damage brain tissue. Such protective specializations comprise the Blood-Brain Barrier (BBB), which is made up of multiple cells that insulate and support proper exchange between the blood and surrounding tissue. This specialized vasculature in the brain is just one example of organ-specific vascular diversity in the body.

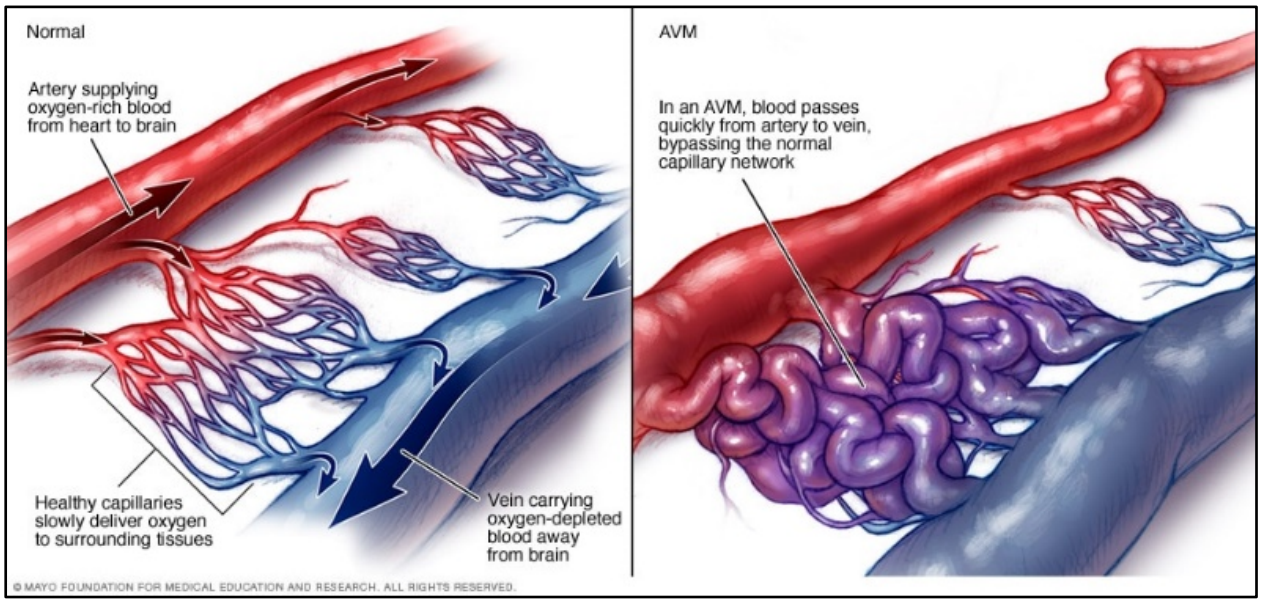

Figure 1. Diagram of normal vascular structure compared to that in AVM (Brain AVM (arteriovenous malformation) - Symptoms and causes)

Improper organization of blood vessels can disrupt vascular homeostasis. Arteriovenous malformation (AVM) occurs when the connections between arteries and veins are abnormal (Figure 1). The typically small capillaries are replaced by larger vessels that make a direct connection. This connection causes blood to flow with high pressure and low resistance, which leads to dilated, weakened vessels and likely insufficient gas exchange. These abnormal connections are also prone to forming a tangled mass, known as a nidus (Figure 2). Brain AVM is particularly dangerous, as dilated vessels may rupture, and disrupted blood flow may restrict oxygen delivery to adjacent tissue, leading to neurological deficits.

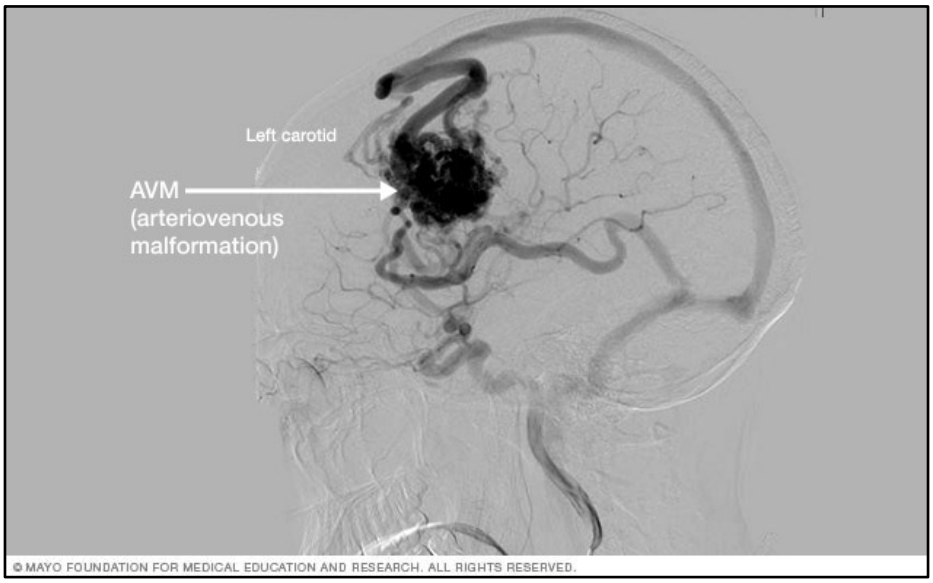

Figure 2. AVM shown on an angiogram (Brain AVM (arteriovenous malformation) - Diagnosis and treatment - Mayo Clinic)

AVM in Humans

Brain AVM is a rare human disease whose underlying causes are not well understood. It is estimated that brain AVM affects about 0.01% of the general population, but it is difficult to get an accurate number of cases because it is often asymptomatic (Friedlander, 2007). AVM is also almost always sporadic, but there are several known genetic mutations that cause AVM,

including germline mutations that lead to Hereditary Hemorrhagic Telangiectasia (HHT). HHT is caused by an autosomal dominant mutation in genes involved in the TGF-β developmental signaling pathway (Guttmacher et al., 1995). HHT is characterized by frequent nosebleeds, abnormal blood vessels of the skin, and AVMs on major organs (Park et al., 2009). Animals models of HHT have suggested that the mutation creates a predisposition for vascular abnormalities, but AVMs are more likely to form when there is vascular injury or a somatic mutation – a "second hit" (Park et al., 2009). Thus, an AVM could result from an irregularity in the vascular repair mechanism. While AVM can occur anywhere in the body, my thesis focuses on AVM within the brain.

There are several clinical signs and symptoms of brain AVM, and these include impairment to cerebral blood vessels and to surrounding brain tissue. Between 42% and 72% of AVMs will hemorrhage, possibly leading to hemorrhagic stroke, and brain AVMs account for 2% of all strokes (Friedlander, 2007). Microhemorrhages, or leakage from blood vessels, can also occur but often go undetected (Abla et al., 2015). Other signs of brain AVM include seizures, migraines, and neurological deficits (Friedlander, 2007). There is currently debate on how AVM can cause neurological deficits. Since a nidus and/or AV shunt may displace a network of capillaries, cerebral blood flow does not cover the same surface area that a healthy vascular network would. One proposed mechanism, vascular steal, states that there could be areas of tissue that do not receive enough blood to function properly, because an AVM diverts flow elsewhere (Mast Henning et al., 1995). Another proposed mechanism is that the enlarged vessel connection or nidus compresses surrounding brain tissue, impairing proper neural function (Sheth and Bodensteiner, 1995). A third possibility is that blood is flowing at such high pressure through an AVM that gas and nutrient exchange is unable to take place, leading to hypoxia in

surrounding tissue (Friedlander, 2007). It is also possible that the symptoms and deficits are caused by a combination of the three proposed effects. Patients can present with any level of any of the symptoms associated with AVM, so there is a range of severity and symptoms associated with this vascular abnormality.

Treatment/Management

Table 1: Spetzler-Martin Grading Scale for AVMs.

Characteristic	Number of points assigned
Size of AVM	
Small (<3 cm)	1 point
Medium (3–6 cm)	2 points
Large (>6 cm)	3 points
Location	
Noneloquent site	0 points
Eloquent site*	1 point
Pattern of venous drainage	
Superficial only	0 points
Deep component	1 point

*Sensorimotor, language, visual cortex, hypothalamus, thalamus, internal capsule, brain stem, cerebellar peduncles, or cerebellar nuclei.

Figure 3. Spetzler-Martin Grading Scale for AVM (Ajiboye et al., 2014)

Diagnostic tools and treatment options for brain AVM are limited. When asymptomatic, AVM often go undetected. When symptoms are shown, imaging techniques are often used to visualize vascular abnormalities, which can help identify the size and location of the brain AVM. Once a patient has been diagnosed with AVM, treatment usually one of two options –

management of symptoms or invasive surgical methods. In severe cases, when the malformation is at a high risk of hemorrhage, surgical resection, radiosurgery, and embolization are options for treatment (Mohr et al., 2014). The risk of hemorrhage increases with increasing patient age, AVM depth in the brain, and draining vein depth (Stapf et al., 2006). There is also a grading system for brain AVM to describe the severity of the abnormality and likely treatment outcome (Figure 3). This system is on a scale of I-V, I being the least severe and V being the most. This scale takes into consideration size of AVM, severity of the deficit if the brain region is damaged, and depth of venous drainage (Spetzler and Martin, 1986). As the grade increases, the risk associated with surgical intervention increases. The scale is meant to be used by physicians to help determine whether an invasive approach is appropriate for a given patient. One clinical trial has shown, however, that the risk associated with interventional therapy for brain AVM outweighs the risk of hemorrhage in any circumstance (Mohr, 2015). Another longitudinal clinical trial is currently underway, to validate or refute this finding (Teo et al., 2015). The care team of a patient with brain AVM, which can include general practice physicians, neurosurgeons, neurologists, neuroradiologists, psychologists, and other specialists, must balance the risk of hemorrhage with the risk of deficits or damage involved in invasive intervention based on their own experience and current research.

Notch Signaling

The Notch signaling pathway is a highly conserved juxtacrine signaling pathway. In mammals, there are four Notch receptors, NOTCH1, NOTCH2, NOTCH3, and NOTCH 4 (Gridley, 2010). These receptors interact with transmembrane protein ligands JAG1, JAG2, DLL1, DLL3, and DLL4. When the Notch ligand and receptor interact, two cleavages occur, first by TACE, also

known as ADAM17, which releases Notch extracellular domain (NECD) and second by γ-secretase, which releases the Notch intracellular domain (NICD) to the cytosol. NICD is transported to the nucleus, where it forms a complex with several transcription factors, including Recombination signal Binding Protein for immunoglobulin kappa J (Rbpj). In endothelial cells, the cells that line blood vessel walls, this complex initiates transcription of several downstream target genes, including *ephrinB2, Neuropilin1, DII4, Hes1,* and *CXCR4,* which indicate that the cells are taking on an arterial identity (Gridley, 2010) (Figure 4).

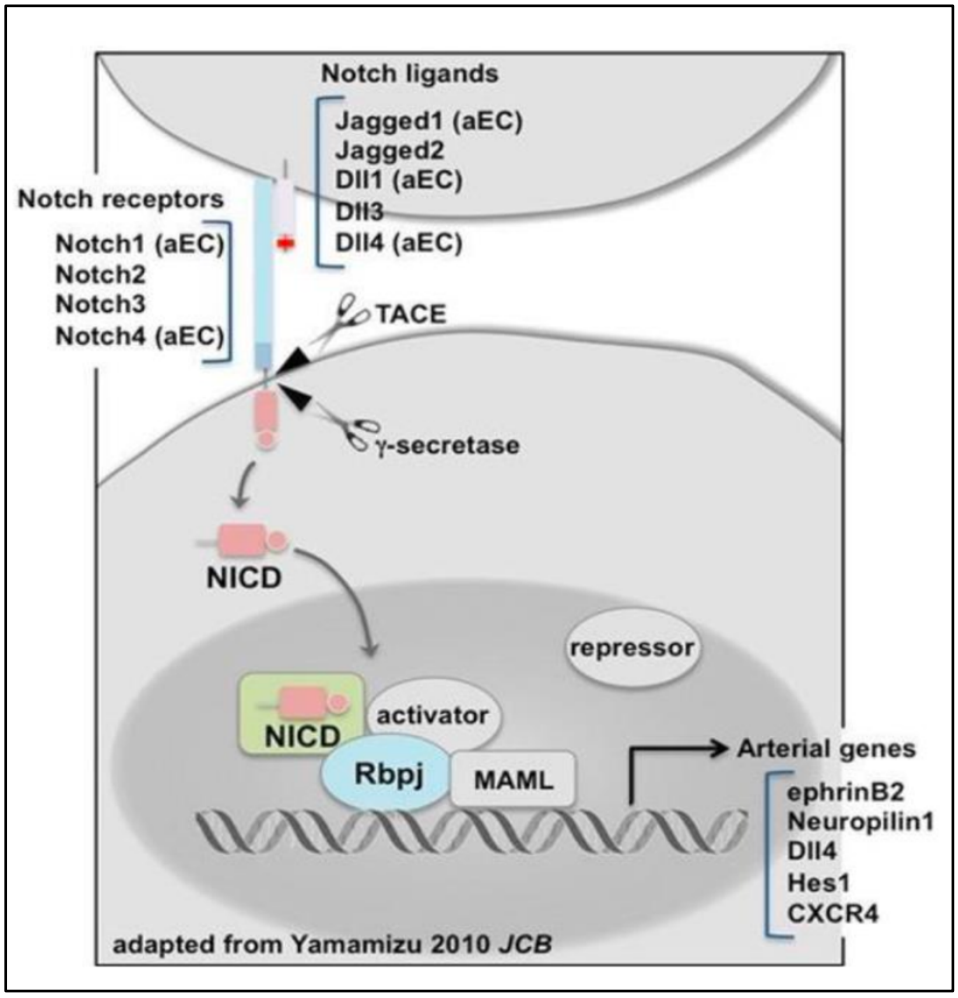

Figure 4. Molecular mechanism of Notch signaling pathway.

While there are several pathways that play a role in angiogenesis, or the development of new blood vessels from existing vasculature, the VEGF and Notch signaling pathways are some of the most studied (Udan et al., 2013). The Notch signaling pathway plays a role in formation of tip cells (Lawson et al., 2001). Tip cells are cells at the end of sprouts from existing vessels that sense the environment to guide growth and formation of new capillary beds (Gridley, 2010). The importance of Notch in arterial/venous differentiation and evidence from human brain AVM samples that show an increased expression of Notch signaling molecules indicate that abnormal Notch signaling may play a role in AVM (ZhuGe et al., 2009). It has been shown experimentally

in mice that both blockade or activation of Notch signaling can cause abnormal arteriovenous connections that resemble AVM (Krebs et al., 2004; Murphy et al., 2008). The transcription factor Rbpj complexes with the NICD to activate transcription and is essential for the downstream genes to be expressed (Yamamizu et al., 2010). The gene for this transcription factor, *Rbpj*, is the target for mutagenesis in a mouse model of brain AVM. Induced deletion of *Rbpj* in endothelial cells at birth causes vascular abnormalities characteristic of AVM to develop (Nielsen et al., 2014) (Figure 5 A-B). As I am interested in understanding how changes in Notch signaling influence AVM formation, I am using this induced endothelial deletion of *Rbpj* as the mouse model of AVM in my thesis.

AVM Mouse Model

Deletion of *Rbpj* in mouse endothelial cells is carried out using an inducible Cre-loxP system (Figure 5). Part of the *Rbpj* gene is flanked by *loxP* sites. The *loxP* sites are recognized by a Cre recombinase protein, and the flanked genetic sequence is excised. To have temporal control over when *Rbpj* is deleted, we use a modified Cre that is fused to a mutated estrogen receptor ($CreER^{T2}$). When tamoxifen, a synthetic ligand to the estrogen receptor, is administered, $CreER^{T2}$ is released from sequestration in the cytoplasm and can reach nuclei where it will act as a recombinase protein. This AVM model is also tissue specific because $CreER^{T2}$ is controlled by a *Cdh5* promoter. *Cdh5* is exclusively expressed in endothelial cells, so *Rbpj* is deleted in endothelial cells. Mutant mice in this model of AVM have the genotype $Cdh5\text{-}CreER^{T2};\ Rbpj^{fx/fx}$, and control mice will be $Cdh5\text{-}CreER^{T2};\ Rbpj^{fx/+}$(Figure 5 C). Both control and mutant mice received tamoxifen injections at postnatal day (P) 1 and P2 to ensure that the recombinase protein and tamoxifen are not confounding variables (Nielsen et al., 2014).

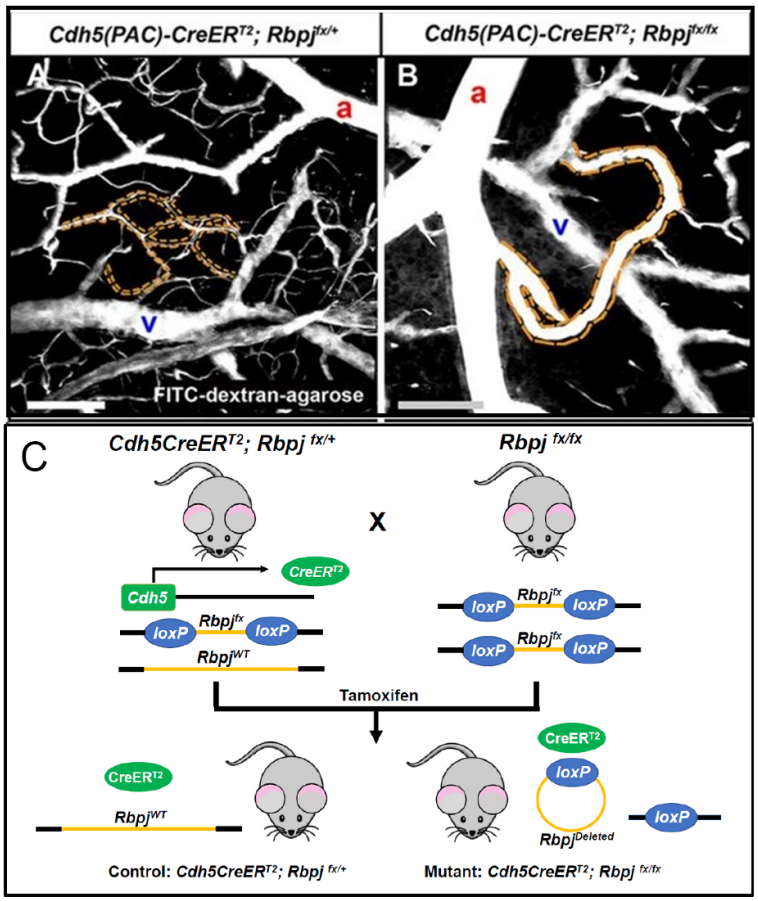

Figure 5. CreER^{T2}-dependent, endothelial Rbpj-deficient model of AVM. (a) Image depicting capillary network of *Cdh5-CreER^{T2}; Rbpj$^{fx/+}$*Control mouse brain (Adapted from Nielsen et al., 2014). (b) Abnormal arteriovenous connection in *Cdh5-CreER^{T2}; Rbpj$^{fx/fx}$* mutant mouse brain. (c) CreER^{T2}-dependent endothelial *Rbpj* deletion mouse model mating scheme (Selhorst, 2019).

Neurovascular Unit

The neurovascular unit is a multicellular structure in the brain that provides insulation and support to microvessels; it is made up of endothelial cells, pericytes, and astrocytes (Hawkins and Davis, 2005) (Figure 6). There is cooperation and communication between cell types within the neurovascular unit. These interactions are vital to proper brain development, to blood-brain barrier function, and to repair after injury (Bell et al., 2020). For example, communication between glial progenitors and blood vessels play a role in astrocyte differentiation and communication between endothelial cells and astrocytes plays a role in proper angiogenesis (Ma et al., 2012; Zerlin and Goldman, 1997). There is also evidence of communication from neurons to endothelial cells, which promotes revascularization in cases of ischemia, and communication from endothelial cells to neural stem cells, which regulates their

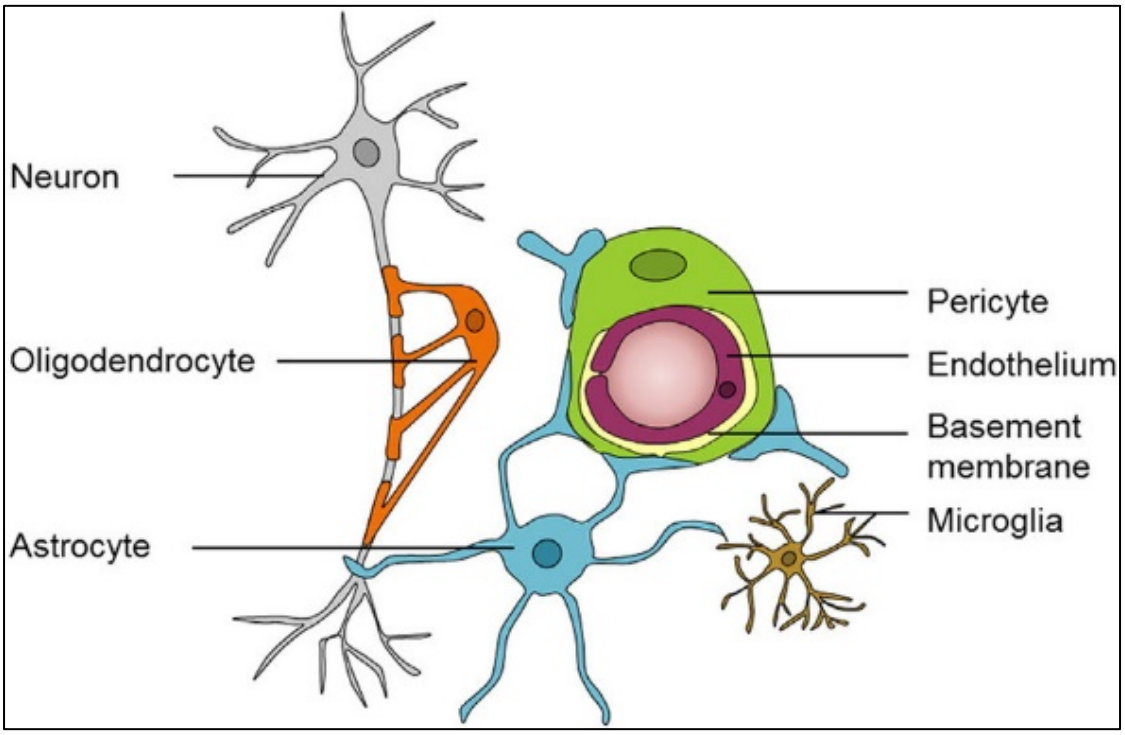

Figure 6. Neurovascular Unit Diagram (Nelson et al., 2016)

growth (Sato et al., 2017; Wei et al., 2015). Xi et al., (2015) observed that neural migration could be guided by vasculature in the cerebellum. There is even evidence of Notch signaling between endothelial cells and astrocytes that upregulates GLT-1, a transporter that is important to glutamate homeostasis (Lee et al., 2017). With the cells of the neurovascular unit in such close association and evidence of intercommunication in repair mechanisms, it is important to consider how manipulation of one cell type could affect the others.

Astrocytes

Astrocytes are known to provide support to neurons, but they also provide significant aid to brain vasculature. Astrocytes are vital to insulation of the neurovascular unit and play important roles in development and regulation of blood vessels in the brain. Specifically, astrocytes are required for proper microvessel growth. Major blood vessels are present in the brain before astrogliogenesis and there is evidence that endothelial cell signaling is necessary for glial precursor cells to differentiate into astrocytes (Imura et al., 2008). Once astrocytes are present, however, they are important for formation of vessel branches and connections. When normal astrocyte function is suppressed in mice, vessel sprouting is unstable, so proper capillaries cannot form from existing vessels (Ma et al., 2012). Astrocytes also are involved in regulating dilation of vessels in response to oxygen demand from nervous tissue (Koehler et al., 2006). There is a great deal of cooperation between astrocytes and blood vessels; astrocytes play a significant role in the neurovascular unit and contribute to support and development of brain vasculature. The endfeet of astrocyte projections also surround microvessels and provide some barrier function at this level. This is known as the glia limitans. However, the role of astrocytes and/or the consequences to astrocytes in brain AVM are not understood.

There are several different types of astrocytes throughout the brain that serve varying roles based on the needs of the surrounding nervous tissue. Fibrous astrocytes contain longer, straighter processes and are present in white matter. Fibrous astrocytes also associate with capillaries to form the glial limiting membrane and with nodes of Ranvier on the axon (Kim et al., 2019; Oberheim et al., 2012; Tabata, 2015) (Figure 7A). Protoplasmic astrocytes are present in gray matter and have long, complex branches of processes which form glia limitans and ensheath synapses (Kim et al., 2019; Tabata, 2015) (Figure 7B).

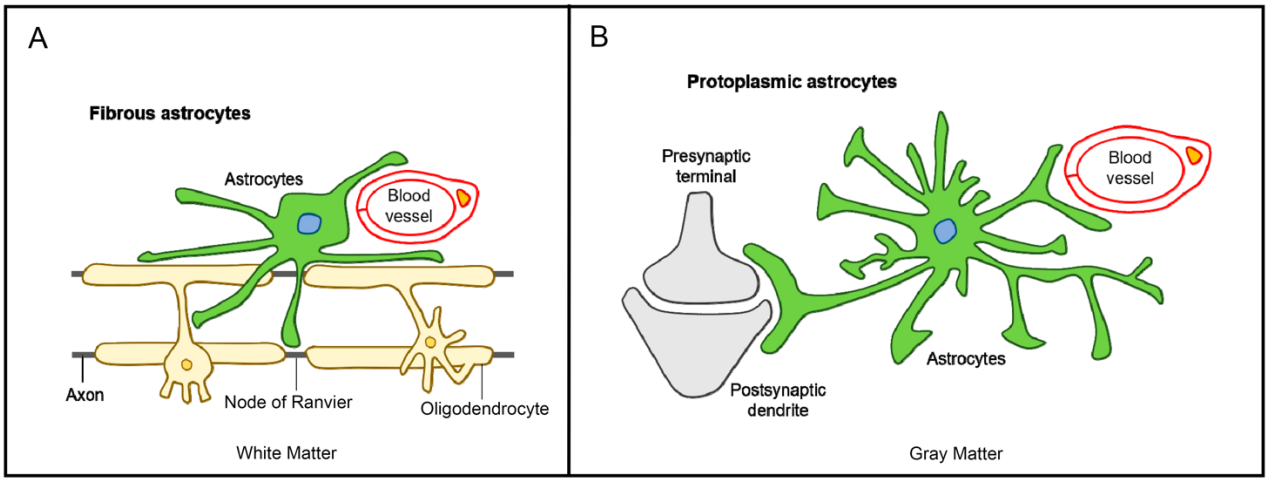

Figure 7. Diagram of fibrous and protoplasmic astrocytes. (a) Fibrous astrocytes are in the white matter and associate with axons and capillary blood vessels. (b) Protoplasmic astrocytes in the gray matter associate with capillary blood vessels and synapses. (adapted from Kim et al., 2019)

In the cerebellum specifically, there are unique astrocytes in the molecular and granule layer. In the molecular layer, there are Bergmann glia (Figure 8). Bergmann glia are a form of semi-radial, unipolar protoplasmic astrocytes with long projections that wrap Purkinje cell

dendrites (Yamada and Watanabe, 2002). In the granule layer, there are velate astrocytes (Figure 8). Velate astrocytes are a type of protoplasmic astrocyte that surround granule cell neurons (Stevens and Muthukumar, 2016).

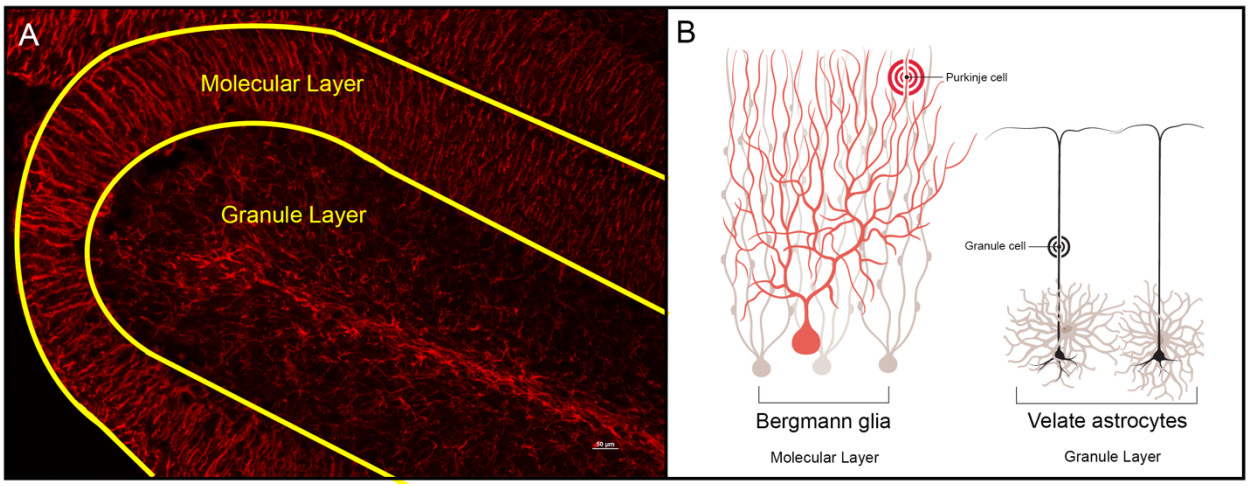

Figure 8. Astrocytes in the cerebellum. (a) GFAP stained image of cerebellum with molecular and granule layers labeled. (b) Diagram depicting astrocytes of the molecular and granular layer and the neural cells they associate with (adapted from Stevens and Muthukumar, 2016).

Reactive Astrogliosis in Disease and Injury

Reactive astrogliosis occurs when glial cell homeostasis changes, in response to injury in the brain – either traumatic brain injury or neurological/neurodegenerative disease. While there are varying reports of how to define reactive astrocytes, in terms of morphological and molecular alterations, there are several defining attributes of a reactive astrocyte. Reactive astrocytes tend to undergo 1) proliferation, or cell division; 2) hypertrophy, or an increase in the diameter of the cell body and processes; 3) increased expression of glial fibrillary acidic protein (GFAP); and 4) polarization, where processes are extended toward compromised tissue (Bardehle et al., 2013). Previously, reactive astrocytes caused by neuroinflammation and ischemia were classified as A1

and A2, respectively. Those categories of reactive astrocytes were primarily based on differential gene expression, which were predictive of different functions. A1 reactive astrocytes were known to have more damaging effects to neurons, whereas A2 astrocytes were thought to release neurotrophic factors, or factors that promote neuron growth and survival. (Liddelow and Barres, 2017; Liddelow et al., 2017; Shinozaki et al., 2017). Recently, however, a multi-lab, multi-institute group of astrocyte researchers has established and published new guidelines for the study of reactive astrocytes. This group has deemed the separation of astrocytes into only two categories to be insufficient to accurately encompass the diversity of reactive astrocytes, which can have varying levels of reactivity and neuroprotection/neurotoxicity (Escartin et al., 2021). These guidelines outlined molecular markers, such as GFAP and C3, and functional assessments, like proliferation analysis and blood-brain barrier integrity detection, to be used to characterize astrocyte phenotype and potentially qualify astrocytes as reactive (Escartin et al., 2021). The characteristics of reactive astrocytes can impact the ability of neural tissue to heal from damage. Increased expression of astrocytic pro-inflammatory factors was observed in Huntington's Disease, Alzheimer's Disease, ALS, and Multiple Sclerosis, indicating possible neurotoxic astrocyte reactivity (Liddelow et al., 2017). It has also been observed that reactive astrocytes express neuroprotective factors in ischemic stroke (Becerra-Calixto and Cardona-Gómez, 2017; Choudhury and Ding, 2016; Shimada et al., 2011). Altered expression of select transcripts may help to discern whether reactive astrocytes are more neuroprotective or neurotoxic (Yun et al., 2018); however, additional features of reactive astrocytes should be described during investigation into pathological astrocyte reactivity.

Astrocytes in Brain AVM and Hypothesis

There is currently limited research on astrocytes and brain AVM; in fact, astrocyte reactivity has not been comprehensively described in human brain AVM or in mouse models of brain AVM. There has been speculation that astrocytes may play a role in overactive VEGF signaling related to brain AVM (Li et al., 2018). Existing research focuses primarily on effects within endothelial cells and with pericytes, support cells specific to the neurovascular unit. (Tu et al., 2006; Winkler et al., 2018). There has been significant progress toward understanding AVM, but the role of astrocytes in AVM has not been pursued and could produce useful insight. Astrocytes play an important role in capillary formation and blood vessel support, and AVM is a dysfunction in development and repair of arteriovenous connections. Also, it has been demonstrated that Notch 1 signaling plays a role in regulating astrocyte reactivity and there is crosstalk within the neurovascular unit to the astrocytes (Shimada et al., 2011; Wolburg-Buchholz et al., 2009).

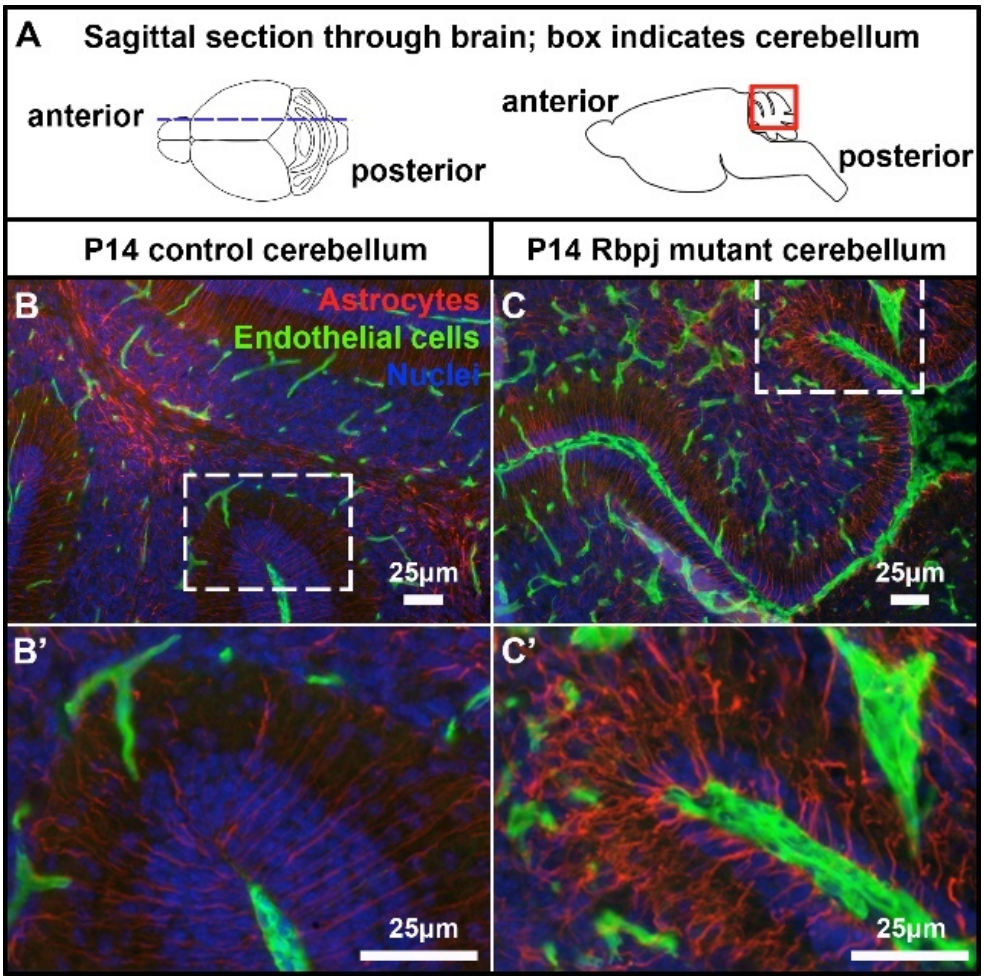

Figure 9. GFAP cerebellum images of Rbpj-mediated AVM model control and mutant. (a) Sagittal sections were stained with antibodies for astrocytes and endothelial cells. (b-b') Control cerebellum astrocytes show thin, straight projections. (c-c') Astrocytes in mutant cerebellum show tortuous, abnormal shape (Unpublished Data, Timothy Wohl, Nielsen Lab)

Unpublished data from the Nielsen lab suggests that in tissue from the Rbpj-brain AVM model, astrocytes appear abnormal (Figure 9). AVM causes stress on neural tissue, so this abnormality may indicate that the astrocytes are reactive. While this may only be a result of dysfunction in endothelial cells, it is worth investigation to determine whether astrocytic abnormalities are a cause or effect of AVM. Even if abnormal astrocyte function is only a consequence of brain AVM, it could be of clinical importance to find out if there is further risk

or damage to be assessed. **I have tested the hypothesis that, as a consequence of Rbpj-mediated brain AVM, astrocytes acquire characteristics of reactivity, including morphological change, increased proliferation, polarization toward damaged vessels, and altered molecular expression.** I report the following major findings:

1. Width of astrocyte projections significantly increased in Rbpj mutant cerebellum, as compared to controls.
2. Number of cells double-positive for GFAP and EdU significantly increased in Rbpj mutant cortex, as compared to controls.
3. GFAP-positive tissue area did not change in cortex, cerebellum, or brain stem; however, results trended toward an increased GFAP-positive area in mutant cerebellum and cortex, as compared to controls.
4. An enriched astrocyte population was isolated from control and mutant mouse brain. Quantitative real-time PCR showed successful amplification of products from *β-actin*, *Gfap*, *Aldh1L1*, and *C3* transcripts, the latter three being astrocyte specific transcripts. This will allow future assessment of transcripts that could provide more insight into astrocyte reactivity in the Rbpj model of AVM.

METHODS:

Mice

Experiments were performed in accordance with Institutional Animal Care and Use Committee (IACUC) protocol 16H024. Mice were housed and treated in accordance with IACUC guidelines. The mouse lines *Cdh5-CreER^{T2}* (Sörensen et al., 2009) and *Rbpj^{flox}* (Tanigaki et al., 2002) were provided by Taconic Biosciences (Rensselaer, New York) and Tasuku Honjo (Kyoto University), respectively. *Cdh5-CreER^{T2}; Rbpj^{fx+x}* control and *Cdh5-CreER^{T2}; Rbpj$^{fx/fx}$* experimental mice were injected on P1 and P2 with 100 µg of Tamoxifen (Sigma) in 50 uL of peanut oil (Planters) intragastrically (Nielsen et al., 2014).

Genotyping

Mice were genotyped to determine controls from mutants. Genotyping was carried out using fluorescence or polymerase chain reaction (PCR) and gel electrophoresis. 1-2 mm tail biopsies were collected from each mouse. *Rosa$^{mT/mG}$* genotype was determined, based on whether the sample was positive for mTomato fluorescence (Nikon NiU microscope) or by PCR based method (follows). To determine the *Rbpj* and *Cre* and *Rosa$^{mT/mG}$* genotypes, first, DNA was extracted through the following steps. 200 uL of 50 mM NaOH was added to a microcentrifuge tube, along with the tail sample. The tube was heated to 95ºC for 25-40 minutes, with 30-60 second vortex in the middle and end of incubation. Tissue was heated and vortexed until completely digested. Then, 50 uL of 1M Tris, pH 8 was added to neutralize, and the mixture was centrifuged at 14,000 rpm for 5 minutes. 1 uL of extracted genomic DNA was used for PCR.

Standard PCR protocol was followed, using Taq polymerase (ThermoFisher) for 40 rounds of amplification and the conditions in Figure 10.

Gene	Primer Sequence	Annealing Temperature	Amplicon Size
Rbpj	FORWARD: ACCAGAATCTGTTTGTTATTTGCATTACTG REVERSE: ATGTACATTTTGTACTCACAGAGATGGATG	56°C	Flox: 350 bp WT: 200 bp
Cre	FORWARD: GCCTGCATTACCGGTCGATGCAACGAGTG REVERSE: ATGTACATTTTGTACTCACAGAGATGGATG	56°C	~400 bp
GFP	FORWARD: TACGGCAAGCTGACCCTGAAGTTC REVERSE: AAGTCGATGCCCTTCAGCTCGATG	65°C	433 bp

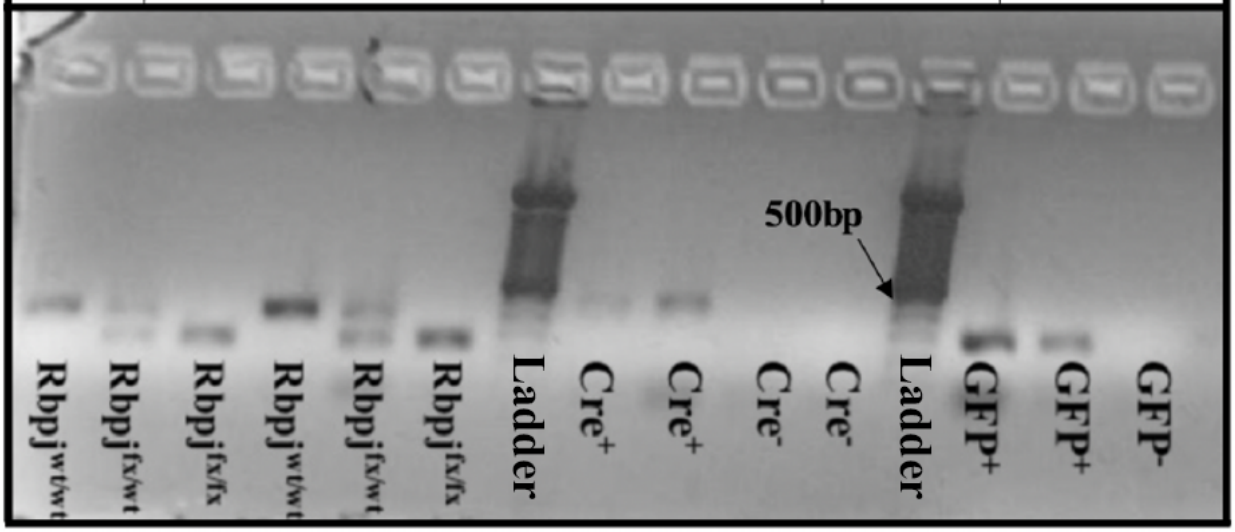

Figure 10. PCR conditions for genotyping and gel electrophoresis from PCR

Cre Responsive Genetic Labeling

For certain experiments, *Rosa26*$^{mT/mG}$ was used as a genetic label for endothelial cells (Figure 11). *Rosa26*$^{mT/mG}$ is a Cre-responsive reporter allele (Muzumdar et al., 2007). This construct expresses mTomato, a red fluorescent protein, whose DNA sequence is knocked into

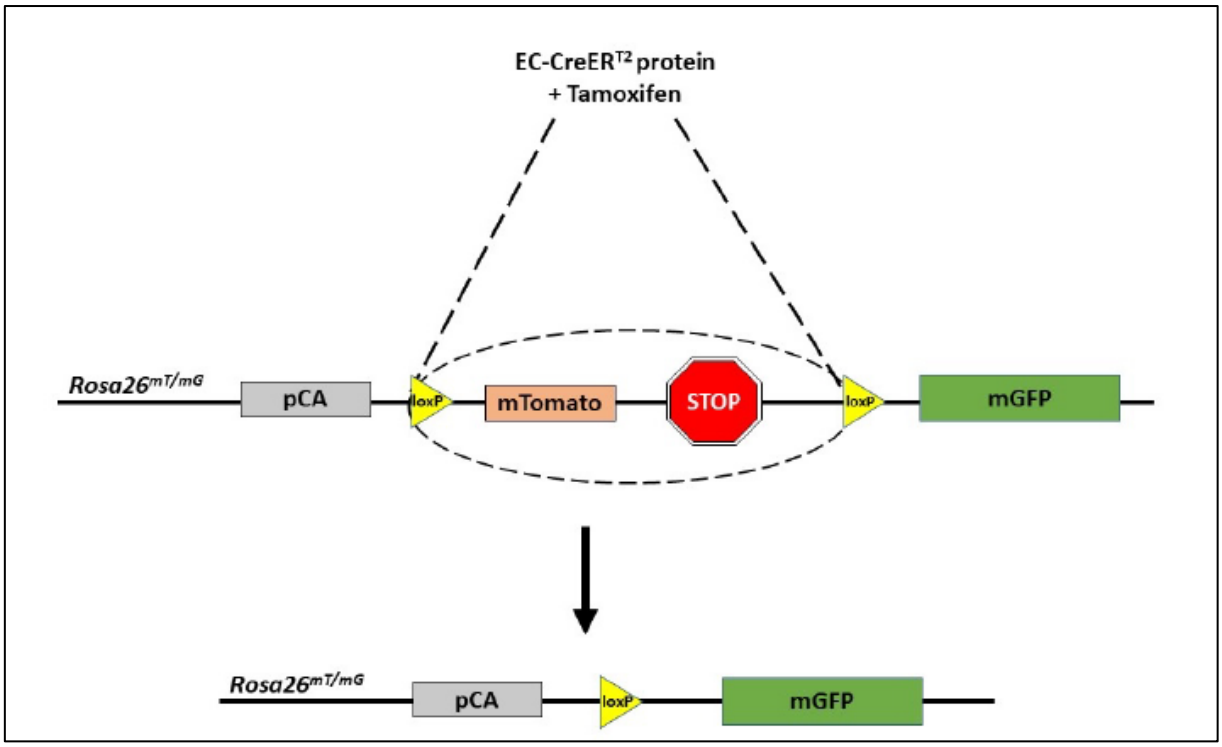

Figure 11. Illustration of the activity of CreER^{T2}-loxP on the *Rosa26*$^{mT/mG}$ allele.

the ubiquitously expressed *Rosa26* locus. Thus, all cell membranes express mTomato, in the absence of Cre recombinase. If Cre is present in endothelial cells, for example, then *mTomato* and a downstream stop cassette are excised, and mGFP, a green fluorescent protein which also targets the membrane, is expressed. In all cells where the *Rosa26*$^{mT/mG}$ allele is recombined, the cell membranes express mGFP (fluoresce green), while all other cell membranes express mTomato (fluoresce red). Since CreER^{T2} requires *Cdh5* promoter for recombinase activity to occur, endothelial cells were labeled with mGFP in the Rbpj model of AVM.

Immunostaining

For certain experiments, endothelial cells and other cells of interest were visualized using a fluorescent tag expressed by a protein specific to the cell type of interest, known as a cell marker (Figure 12). For immunostaining, mice were anesthetized with a vaporized mixture of oxygen and isoflurane. Mice are perfused transcardially with 1% paraformaldehyde (PFA) until they become stiff and vascularized organs became pale, approximately four minutes. The exsanguination that takes place during this procedure is an IACUC approved method of euthanasia. Brain tissue was harvested and fixed in 4% PFA at 4 degrees Celsius overnight. Tissue was rinsed in phosphate-buffered saline solution (PBS) and cryoprotected in 30% sucrose at 4 degrees Celsius overnight. The tissue was then frozen in optimal cutting temperature (OCT) solution in molds on dry ice. Tissue was stored at -80 degrees Celsius until sectioned with a Leica Cryostat CM1950 (Ohio University Histopathology Core) at 10-14 μm thickness.

To achieve cell-specific labeling, indirect immunofluorescence was used. The GFAP primary antibody (Millipore, AB5541) was applied, and fluorophore-conjugated secondary antibodies that recognize primary antibodies were subsequently applied. The resultant fluorescence was visualized using an upright Nikon NiU microscope. Images were captured using Nikon Elements software.

For GFAP images, brain tissue sections were treated with a donkey serum blocking step (Jackson ImmunoResearch), followed by chicken anti-GFAP (1:200, Millipore, AB5541) primary antibody, then donkey-anti-chicken secondary antibody conjugated to Cy3 (1:500, Jackson Laboratories, 703-165-155).

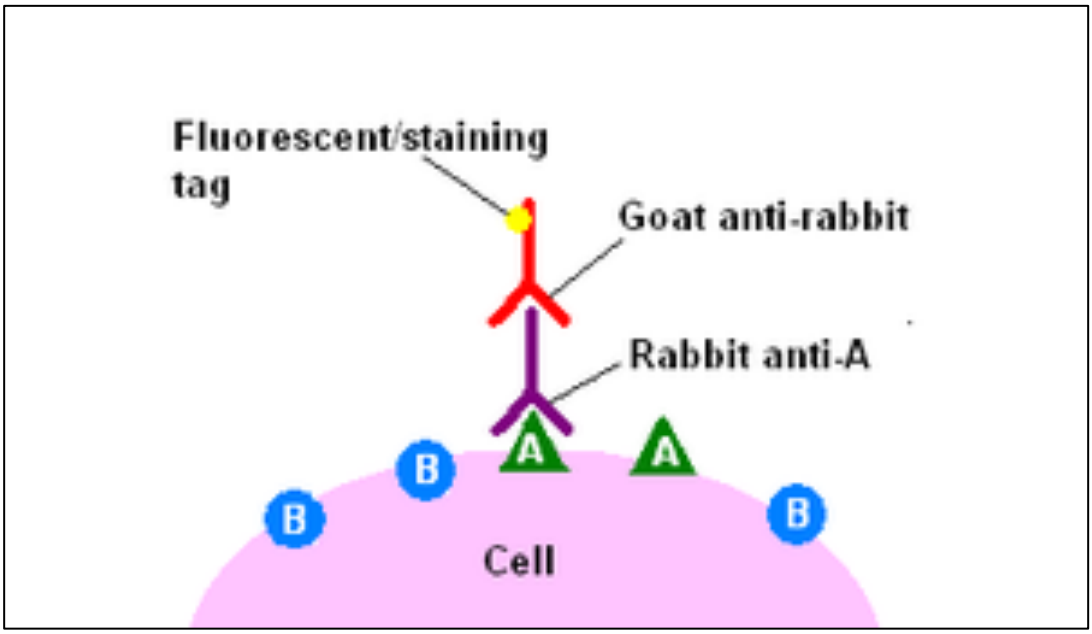

Figure 12. Illustration of indirect antibody immunofluorescence

Proliferation Assay/EdU

Cell proliferation was measured using Click-It™ EdU proliferation kit (ThermoFisher). This kit measures proliferation through the S-phase of the cell cycle. It uses 5-ethynyl-2'deoxyuridine (EdU), which is a nucleoside analog for thymidine and is incorporated during DNA synthesis. A catalyzed covalent reaction takes place between an alkyne group on EdU and a picolyl azide group on Alexa Fluor dye, leaving the two conjugated and able to be detected through fluorescence microscopy.

Pups were injected intraperitoneally with 10 ug EdU/g body weight for 3 days (P12, P13, P14), and brains were harvested 4 hours after the injection on the third day of EdU pulse. Brains were perfused intracardially with 1x PBS and post-fixed in 1% PFA in PBS overnight. Brains were then dehydrated in 30% sucrose solution in PBS overnight to prevent formation of ice

crystals. 12 um tissue sections were cut on a cryostat and fixed in 4% PFA in PBS for 15 minutes at room temperature. Sections were then washed in 3% BSA in PBS. Sections were then permeabilized in 0.5% Triton X-100 in PBS for 20 minutes. Then the Click-iT reaction cocktail was prepared and the permeabilization buffer was removed by washing sections with 3% BSA in PBS. Any accompanying antibody staining was performed, as described above, then 100 mL of the Click-iT™ cocktail, prepared as specified by manufacturer instructions, was added to each section. The tissue was incubated for 2x 30 minutes, away from light, then washed with 3% BSA in PBS, washed again with 1X PBS, stained with DAPI for 5 minutes to label DNA, washed with 1X PBS, and mounted with Prolong Gold (Fisher Scientific) under glass coverslips.

Western Blot

Western Blot was performed by taking a sample of brain tissue and isolating and separating the proteins within the tissue. Whole sample brains were homogenized by adding a tissue lysis buffer made of Tris-HCl, $MgCl_2$, NaCl, 1% NP-40, 0.1% SDS, and protease inhibitor. Next, the lysate is sonicated and centrifuged. Proteins were separated by size using 8% sodium dodecyl sulphate–polyacrylamide gel electrophoresis (SDS-PAGE) and transferred from the gel onto a PVDF blotting membrane via wet transfer for 3 hours. The membrane then was treated with blocking solution and incubated with various primary antibodies, which bound to protein antigens of interest. The primary antibodies used were chicken anti-GFAP (Millipore, AB5541) and mouse anti-Aldh1L1 (Millipore, MABN495). The membrane was incubated with appropriate horseradish peroxidase (HRP)-conjugated anti-chicken and anti-mouse secondary antibodies (Jackson ImmunoResearch). Protein bands were then visualized with BioRad Gel Doc Imaging System and digitally imaged and analyzed with ImageLab software.

Astrocyte Cell Isolation

Astrocytes were isolated through magnetic-activated cell sorting (MACS), with an astrocyte-specific antibody. MACS is a cell sorting method that uses antibody-bound magnetic beads to bind target antigens and capture antigen-expressing cells inside a column, placed between magnets. To isolate astrocytes, mice were decapitated at P14, in accordance with IACUC protocol 16H024. Brains were harvested and minced and triturated with Milltenyi enzyme mix (130-107-677) in a petri dish. The tissue was incubated in the enzyme mix at 37 degrees Celsius for 45 minutes, with periodic trituration. The tissue-buffer mixture was suspended by trituration, strained with a 40 μm strainer, centrifuged at 300 g for 10 minutes, and decanted. Then, the suspension was run through a Percoll gradient (GE Health) to remove myelin. The remaining sample was centrifuged at 400 g for 30 minutes, washed, and the pellet was collected.

For the MACS separation step, the sample was centrifuged at 300 g for 10 minutes, and the supernatant was aspirated into a waste container. The remaining sample was incubated in FcR Blocking Reagent (Miltenyi) at 4 degrees Celsius. Then, Anti-ACSA-2 MicroBeads (Miltenyi) were added, mixed, and incubated at 4 degrees Celsius for 15 minutes. The mixture was then washed, centrifuged at 300 g for 10 minutes, aspirated, and resuspended. A column was placed within the magnetic field of a MACS Separator. The column was primed with a MACS-specific buffer made of FBS and EDTA in 1% PBS at pH 7.4 and the cell suspension was applied. The column was then washed with buffer to wash out cells not bound to antigen on magnetic beads. The column was removed from the separator, and remaining cells were eluted with the MACS buffer and a plunger. This final elution contained ACSA-2-positive astrocytes.

qPCR

Quantitative real-time PCR **(**qPCR) was performed to analyze relative levels of transcript expression in tissue of interest. Total RNA was isolated from cells, using a QIAGEN RNeasy Plus Micro kit. Next, cDNA was prepared from total RNA with reverse transcriptase and random hexamer primers (Invitrogen). Concentration of total RNA and cDNA were measured using a Nanodrop spectrophotometer. The cDNA, along with appropriate primers (Eurofins Genomics), outlined below in Table 1, were loaded into a BioRad thermal cycler, which rapidly changed temperature within the samples, while a beam of light detected fluorescence emitted by the excited fluorophore. The fluorescence was measured repeatedly, while the temperature/amplification cycles took place. The ΔΔCt method was used to determine relative abundance, between control and mutant samples at a given time, which indicated that the level of transcript expression in the isolated astrocytes from mutant vs. control mice.

Primer	Forward	Reverse
H2-T23 (Histocompatibility 2, D region locus 3)	GGACCGCGAATGACATAGC	GCACCTCAGGGTGACTTCAT
Serpin G1 (Serpin family G member 1)	ACAGCCCCCTCTGAATTCTT	GGATGCTCTCCAAGTTGCTC

H2-D1 (histocompatibility 2, D region locus 1)	TCCGAGATTGTAAAGCGTGAAGA	ACAGGGCAGTGCAGGGATAG
Gbp2 (Guanylate Binding Protein 2)	GGGGTCACTGGTCTGACCACT	GGGAAACCTGGGATGAGATT
Tgm1 (Transglutaminase 1)	CTGTTGGTCCCGTCCCAAA	GGACCTTCCATTGTGCCTGG
Ptx3 (Pentraxin 3)	AACAAGCTCTGTTGCCCATT	TCCCAAATGGAACATTGGAT
S100a10 (S100 Calcium Binding Protein A10)	CCTCTGGCTGTGGACAAAAT	CTGCTCACAAGAAGCAGTGG
Cd109 (Cluster of Differentiation 109)	CACAGTCGGGAGCCCTAAAG	GCAGCGATTTCGATGTCCAC
C3 (Complement C3)	CCAGCTCCCCATTAGCTCTG	GCACTTGCCTCTTTAGGAAGTC
Il-1a (Interleukin 1 alpha)	GCACCTTACACCTACCAGAGT	AAACTTCTGCCTGACGAGCTT

C1q (Complement C1q A Chain)	TCTGCACTGTACCCGGCTA	CCCTGGTAAATGTGACCCTTTT
TNFα (Tumor Necrosis Factor)	CCCTCACACTCAGATCATCTTCT	GCTACGACGTGGGCTACAG

Table 1. Primers used for qPCR.

Analyses

ImageJ software was used to measure the width of astrocyte projections and to quantify GFAP-positive areas of brain tissue. Four image fields and sixteen projection widths were measured per experimental unit. Three control and three mutants were used for this analysis.

Adobe Photoshop was used to quantify number of cells positive for EdU, GFAP, and DAPI. Five image fields were measured per experimental unit. Three control and three mutant mice were used for this analysis.

For statistical analyses, Graph Pad by Prism software was used. To compare control and mutant data, unpaired T-tests with Welch's correction were run. P values under 0.05 were considered significant (*P < 0.05, **P < 0.01, ***P < 0.001, ns = not significant). Data are reported as [control mean, RbpjiΔEC mutant mean, p value, control N-number, mutant N-number].

RESULTS:

Astrocyte projection diameter increased in cerebellum of P14 Rbpj$^{i\Delta EC}$ mutant mice

The first characteristic of astrocyte reactivity I tested was hypertrophy. To test whether astrocytes underwent hypertrophy in response to endothelial deletion of *Rbpj,* width of astrocyte projections was measured in the cerebellum. The cerebellum provides an advantage to measuring astrocyte hypertrophy, because of the unique morphology of Bergmann glial cells. The long astrocyte projections of these molecular layer astrocytes allow for consistent measurement. Sagittal sections of P14 control and Rbpj$^{i\Delta EC}$ mutant mouse brains were stained with GFAP, fluorescence microscope images were taken in the cerebellum, and astrocyte projection width was measured in ImageJ (Figure 13 A-C'). At this timepoint, astrocyte projection width was increased in Rbpj$^{i\Delta EC}$ mutant cerebellum, as compared to controls. (Figure 13 D) [control: 1.1 μm, Rbpj$^{i\Delta EC}$ mutant: 1.5 μm, p=0.0051, N=4 controls, N=4 mutants]. The increased diameter of astrocyte projections in mutant cerebellum suggests that astrocyte hypertrophy is taking place, following endothelial deletion of Rbpj.

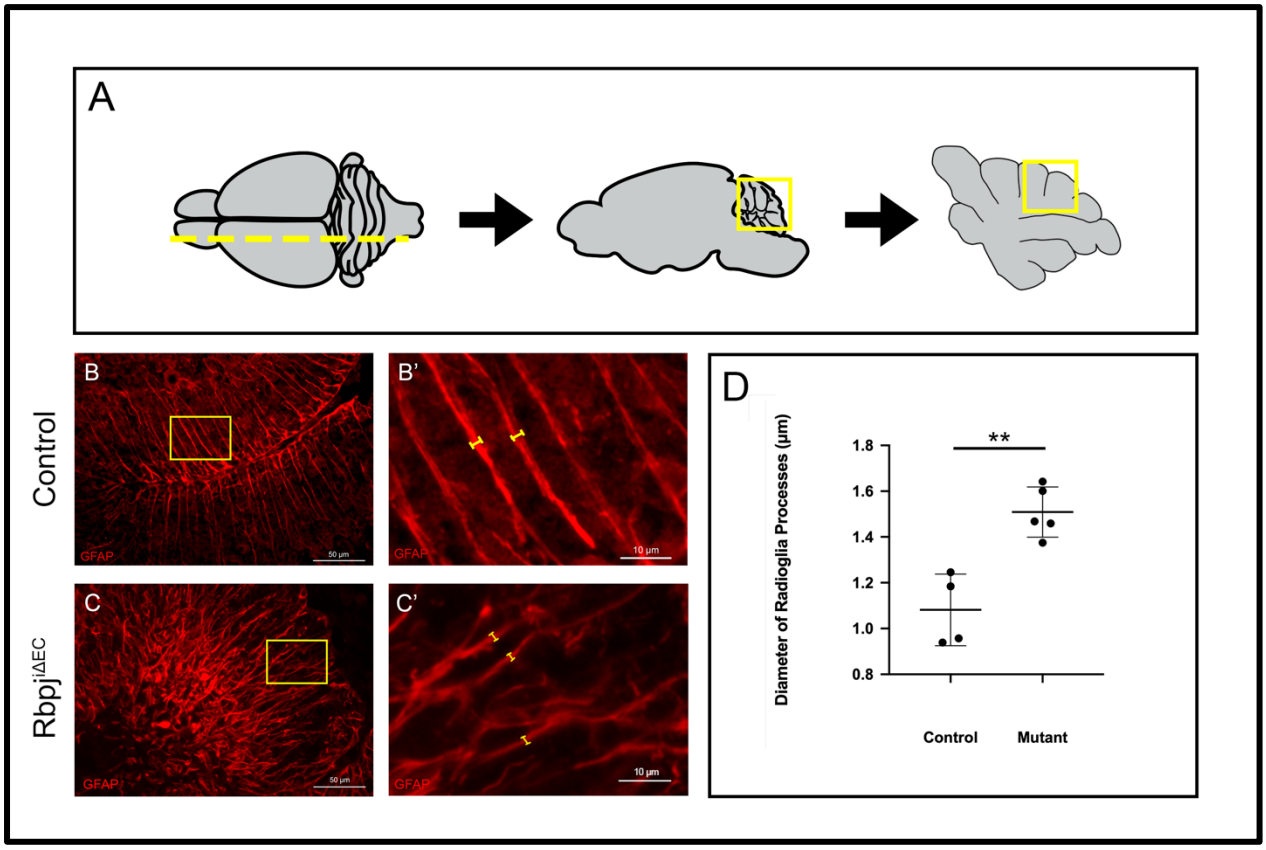

Figure 13. Astrocyte projection diameter increased in P14 Rbpj mutant cerebellum. (a) Diagram depicting sagittal tissue section and cerebellum brain region imaged. (b,c) Sample images and regions of interest for cerebellum Bergmann glia projection measurement. (b',c') Digitally zoomed cerebellum images. Example of astrocyte projection width measurement. (d) Quantification of astrocyte projection width measurement. Astrocyte projection width increased in Rbpj$^{i\Delta EC}$ mutant compared to control: p=0.0051, N=4 controls, N=4 mutants.

Number of GFAP and EdU double-positive cells increased in P14 Rbpj$^{i\Delta EC}$ cortex

The next characteristic of reactive astrocytes I tested was hyperproliferation. To measure whether proliferation increased in Rbpj$^{i\Delta EC}$ mutant astrocytes, as compared to controls, mice were injected with EdU for 3 days (P12, P13, P14), so that proliferating cells could be detected through incorporation of a fluorescent S-phase marker. Sagittal brain sections were stained with GFAP and DAPI to visualize astrocytes and nuclei, respectively (Figure 14 A). Astrocyte proliferation was measured by the number of cells positive for GFAP, EdU, and DAPI per mm^2 of cortex area (Figure 14 B-K). Due to the morphology of astrocytes in the mouse cortex, cell bodies were able to be clearly visualized, allowing for more reliable selection of GFAP and EdU double-positive cells. There were an increased number of EdU positive astrocytes in the mutant cortex, compared to control (Figure 14 L) [control: 1.5, mutant: 7.3, p=0.0009, N=4 controls, N=4 mutants]. Increased number of EdU and GFAP double-positive cells suggests that GFAP+ astrocytes were proliferating in P14 mutant cortex following endothelial deletion of Rbpj.

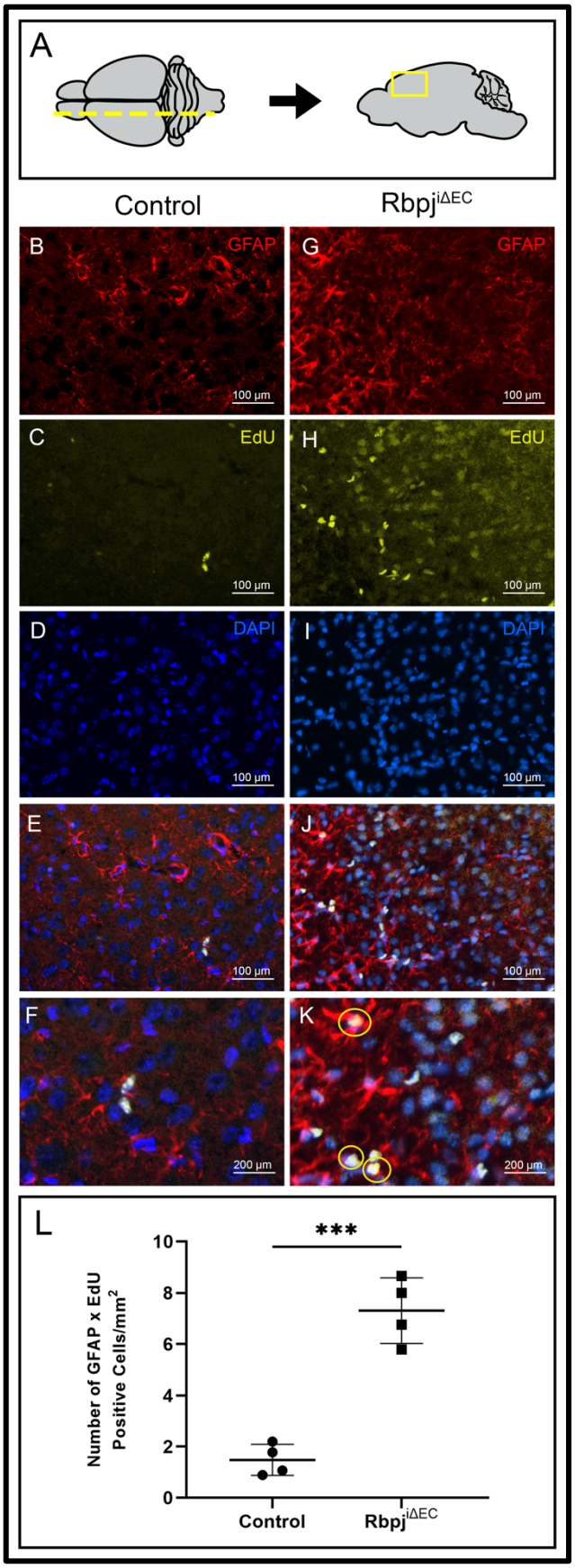

Figure 14. Number of GFAP+/EdU+ cells increased in P14 Rbpj mutant cortex. (a) Diagram depicting sagittal tissue section and cortex region imaged. Tissue was stained with GFAP (b,g), EdU (c,h), and DAPI (d,i). (e,j) Merged image. (f,k) Images digitally zoomed to demonstrate selection of cells positive for EdU, GFAP, and DAPI. (l) Quantification of cells positive for both GFAP and EdU per mm^2 cortex area. Number of GFAP and EdU positive cells increased in Rbpj$^{i\Delta EC}$ mutant compared to control: p=0.0009, N=4 controls and N=4 mutants.

GFAP positive area did not change in mutant cortex, cerebellum, and brain stem

In the Rbpj-mediated model of AVM, abnormal arteriovenous connections do not develop in all brain regions with the same severity (Nielsen et al., 2014); thus, I investigated multiple brain regions to assess whether GFAP expression was spatially regulated among brain regions. To test whether GFAP expression was altered following endothelial deletion of *Rbpj*, GFAP-positive area was measured in microscope images. Sagittal brain tissue sections were stained with GFAP and fluorescence microscope images were taken in the cortex (Figure 15 A), cerebellum (Figure 15 E), and brain stem (Figure 15 I) at a 1 second exposure, and GFAP positive area was measured in NiS Elements BR software by defining a "GFAP-positive" threshold and measuring the area of images that reached and surpassed the threshold. The change in astrocyte area was not significant in the cortex (Figure 15 B-D) [control: 3400 μm^2, mutant: 58000 μm^2, p=0.14, N=3 controls, N=3 mutants] or the cerebellum (Figure 15 F-H) [control: 45000 μm^2, mutant: 96000 μm^2, p=0.11, N=3 controls, N=3 mutants]. In the brain stem, there was no change in GFAP-positive area (Figure 15 J-L) [control: 12000 μm^2, mutant: 15000 μm^2, p=0.79, N=3 controls, N=3 mutants]. None of the three brain regions showed significant changes in astrocyte area. These results suggest that endothelial deletion of Rbpj does not lead to increased GFAP-positive area of brain tissue, regardless of whether arteriovenous shunts are present.

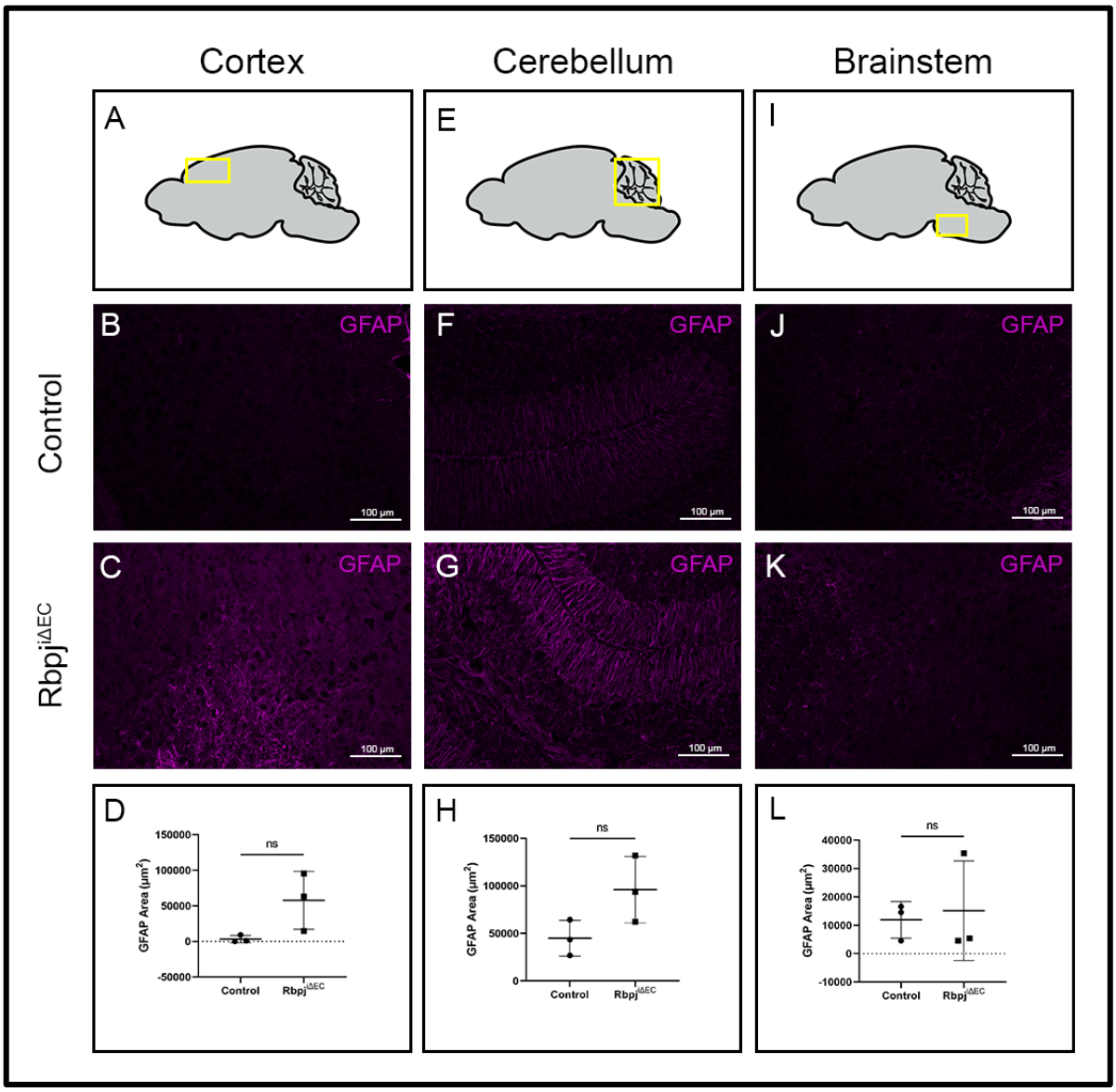

Figure 15. GFAP positive area was not significantly altered in the cortex, cerebellum, or brain stem with endothelial Rbpj deletion. Sagittal tissue sections of P14 brain tissue were stained with GFAP and imaged with a 1 second exposure time in the cortex (a), cerebellum (e), and brain stem (i-l). In the cortex, the increase in astrocyte area from the control (b) to the mutant (c) was not significant. (d) Quantification of cortex astrocyte area analysis: p=0.1438, N=3 controls and N=3 mutants. (f-g) Change in GFAP-positive area in the cerebellum was not significant. (h) Quantification of cerebellum astrocyte area analysis: p=0.1101, N=3 controls and N=3 mutants. There was no significant change in GFAP-positive area in the brain stem from controls (j) to mutants (k). (l) Quantification of brainstem astrocyte area analysis: p=0.79, N=3 controls and N=3 mutants.

Aldh1L1 protein expression did not change in Rbpj mutant

Given that the total area of GFAP-positive tissue did not significantly change following endothelial deletion of Rbpj and given that GFAP is known to be upregulated in reactive astrocytes, I aimed to measure GFAP expression at the protein level. Unfortunately, the attempts to complete a Western blot analysis on GFAP were unsuccessful. Instead, a Western Blot was performed on whole brain tissue from control and Rbpj$^{i\Delta EC}$ mice, using an antibody against Aldh1L1 (Figure 16 A). Aldh1L1 is a universal astrocyte marker and is not reported to be upregulated in reactive astrocytes; thus, Aldh1L1 was used as to compare GFAP expression in control and mutant tissue. As expected, there was no change in Aldh1L1 expression in mutant brain, as compared to controls (Figure 16 B) [control: 0.82 a.u., mutant: 0.57 a.u., p=0.16, N=3 controls, N=3 mutants]. This result suggests that protein expression of Aldh1L1 is not altered by endothelial deletion of *Rbpj*.

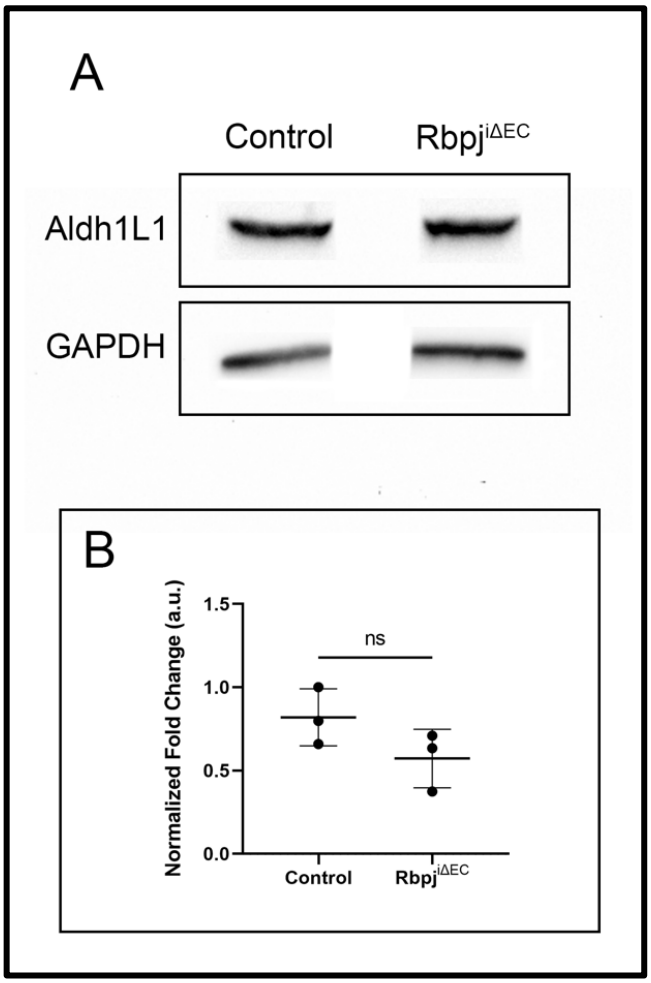

Figure 16. Aldh1L1 protein levels did not change in Rbpj mutant. (a) Aldh1L1 and GAPDH loading control Western blot bands. (b) Quantification of control and mutant levels of Aldh1L1: p=0.16, N=3 controls and N=3 mutants.

Transcript expression did not show significant change in enriched astrocyte cell population of Rbpj mutant

To test whether there were changes in astrocytes on the transcript level in response to endothelial deletion of *Rbpj*, I sought to conduct a quantitative PCR (qPCR) analysis on RNA from isolated astrocytes. I used MACS to separate astrocytes from whole-brain single-cell suspension, and I isolated RNA to be used for analysis. First, I used conventional PCR to complete an enrichment analysis, which revealed that isolated cells expressed astrocyte transcripts *Gfap* and *Aldh1L1* (Figure 17 A). This analysis also revealed that there was very little-to-no contamination by neurons, because the neuronal transcript *Snap25* was amplified to very low levels (Control 1, Mutant 3 in Figure 17 A) or was not detectable (Control 2, Control 3, Mutant 1, Mutant 2 in Figure 17 A), despite 35 cycles, using conventional PCR. For all transcripts, one sample from whole brain was used, as positive control. For all cell samples, expression of *Actb* housekeeping gene *Actb* (β-actin) was used as positive control.

To begin to test for differential transcript expression, between astrocytes isolated from control and mutant brain, I used primers for the transcripts *Gfap*, *C3*, *Aldh1L1*, *s100a10*, and *β-actin*. *Gfap* was used as a marker of astrocyte reactivity, *Aldh1L1* was used as a general astrocyte primer, *C3* was a marker for astrocyte reactivity and had previously been published as an "a1" marker, *s100a10* had previously been published as a marker for "A2" astrocytes, and *β-actin* served as a positive control. None of the primers used showed significant difference between real-time amplification between control and Rbpj-mutant (Figure 17 B), though the fold-change of reactive astrocyte-transcript levels is intriguing and warrants repeating the experiment. These results show successful methodology to enrich for astrocytes and use total RNA from those cells

to complete qPCR experiments. Additional experiments, with larger sample size, are necessary, to determine whether endothelial deletion of Rbpj leads to an alteration in the expression of *Gfap*, *C3*, *Aldh1L1*, and *s100a10 t*ranscripts.

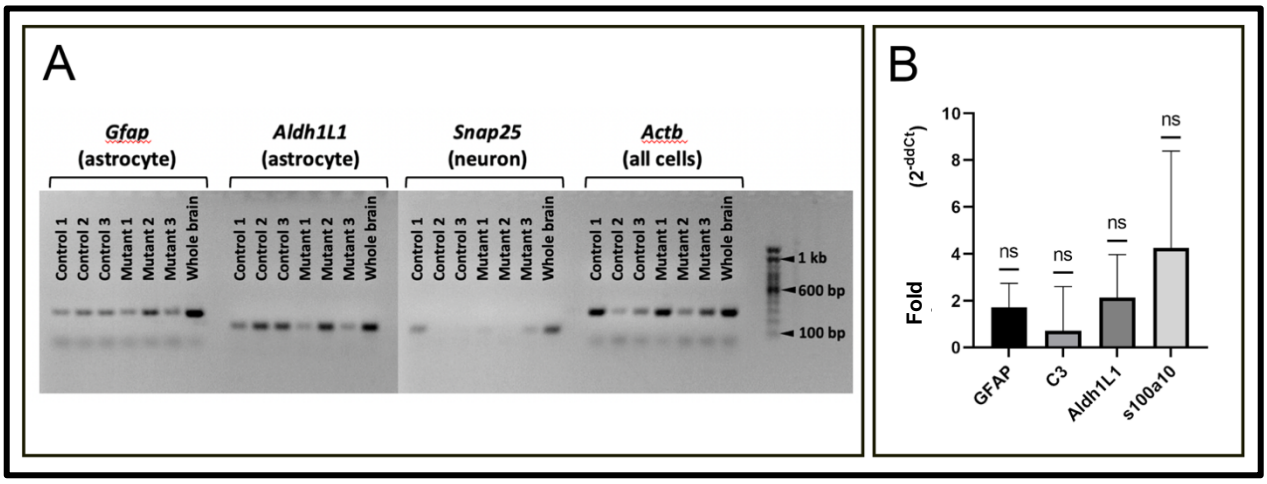

Figure 17. Isolated astrocytes contaminated and transcript levels did not change in Rbpj mutant. (a) Enrichment analysis PCR reaction results. MACS isolation yielded astrocyte-enriched cell population, as evidenced by expression of astrocyte transcripts *Gfap* and *Aldh1L1* and very low expression of neuronal transcript *Snap25*. *Actb* (*β-actin*) was used as positive control. cDNA from whole brain was used as positive control for all transcripts. (b) qPCR analysis showed no significant change in *GFAP*, *C3*, *Aldh1L1*, and *s100a10* in Rbpj mutant, as compared to control.

DISCUSSION:

This thesis is a first step into investigating astrocyte reactivity in Rbpj mediated brain AVM. There is currently little research investigating whether reactive astrocytes are present in AVM models. The goal of this thesis was to gather evidence to suggest whether astrocytes were reactive in the brains of mice in the endothelial Rbpj-mediated model of AVM. Increased astrocyte projection width in the cerebellum and increased proliferation in the cortex are both evidence in support of astrocyte reactivity. Future experiments to analyze expression of factors reported to be associated with astrocyte reactivity are needed, to further understand consequences to astrocytes in the Rbpj model of AVM.

Morphological diversity presents challenges to assessing hypertrophy among astrocytes in different brain regions. The morphology of Bergmann glia in the cerebellum is unique. The presence of long, thin projections allowed for a consistent, reliable way to test for cellular hypertrophy. Beyond the molecular layer of the cerebellum, the morphology of astrocytes becomes irregular. The star shape of velate astrocytes in the granule layer and the astrocytes in the cortex make measuring hypertrophy in other brain regions more difficult. The increase in projection width does provide evidence that astrocytes show hypertrophy in the cerebellum, but it would be useful to assess whether astrocytes in other regions also show hypertrophy in the AVM model mutant.

The same morphology that lends itself to ideal measurement of hypertrophy makes it difficult to count EdU positive astrocytes (Figure 18). The cell body of Bergman glia are typically in line with Purkinje cell bodies as depicted in figure 8. There was a great deal of EdU signal in mutant P14 cerebellum (Figure 18 E), but it is difficult to discern whether an EdU positive cell body belongs to an astrocyte or neuron, because both types of cell bodies are arranged in the same row. Proliferation analyses in the cerebellum could be optimized with a cell-body or nucleus specific astrocyte antibody marker and a neural marker to highlight which EdU positive cell body belonged to which cell. Astrocytes in the mouse cortex, however, showed a distinct cell body when stained with GFAP. This allowed for clearer selection of which cells were positive for EdU in the soma. From this, I found that the number of GFAP and EdU positive cells increased in the Rbpj mutant, as compared to controls. This provides evidence of astrocyte proliferation, a hallmark of astrocyte reactivity, taking place in the cortex.

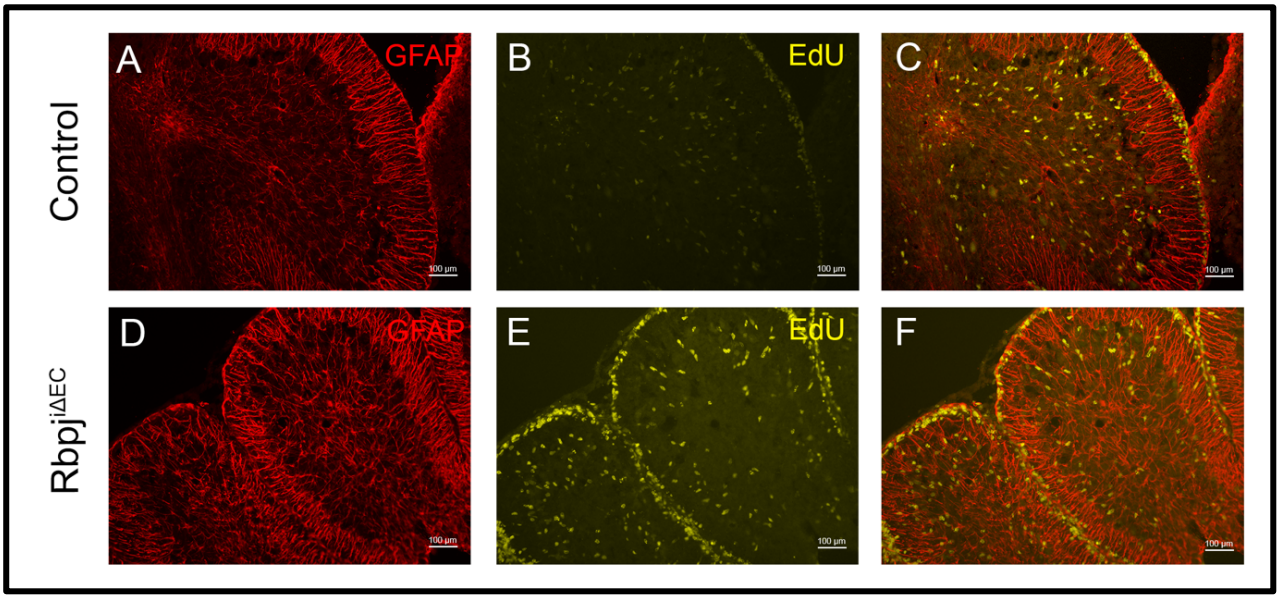

Figure 18. Microscope images of GFAP and EdU cerebellum. Control (a-c) and mutant (d-f) images with GFAP and EdU staining to depict expression in cerebellum. Note: EdU signal is concentrated along edge of molecular layer (b,e).

For astrocyte area analyses, there were not significant changes in GFAP positive area in any of the three brain regions tested. This was expected in the brain stem, because in the Rbpj model of AVM, abnormal vessels are less likely to form in the brain stem (Nielsen et al., 2014). The results followed what was expected, because there was no change in GFAP area with endothelial deletion of *Rbpj*. On the other hand, abnormal vessels are often found in the cerebellum and cortex. There was variability in the results and there were only three controls and three mutants. While the data did not show a significant change, the results from the cortex and cerebellum were trending toward an increase in GFAP area in the Rbpj mutant. This result may raise the question of whether astrocyte reactivity would be localized to the area surrounding abnormal vessels. This would be similar to glial scar formation, which is when astrocytes surround an acute injury as a protective mechanism (Shinozaki et al., 2017). In this case, the abnormal vessel connection may be the "injury" and potential astrocyte reactivity would be localized to the surrounding tissue. I do not believe this is the case, though, because glial scars form in focal injury and deletion of *Rbpj* is a genetic lesion that causes widespread vascular abnormalities. In the Rbpj-mediated model of AVM, there is a range in phenotypic severity, much like how there is variable severity of AVM as it arises in humans. It is possible that, with the range of vascular phenotypes, there could be a range of astrocyte reactivity. In this case, an increased sample size would reveal if there were increased GFAP area in the cerebellum of the Rbpj mutant.

The lack of significant change in GFAP-positive area in the cerebellum, while astrocyte projections in the cerebellum were shown to have increased width, is somewhat contradictory. It is possible that mutant cerebellar astrocytes are reactive, and if the sample number were increased or abnormal vessels were taken into consideration, that GFAP-positive area would

increase in the Rbpj mutant cerebellum. Based on qualitative observation of control and mutant cerebellum, Bergmann glia do appear to be affected by the endothelial deletion of *Rbpj*. I assessed these morphological changes from the lens of astrocyte reactivity, but there could be other factors at play in the mutant cerebellum. Bergmann glia share the molecular layer with Purkinje cells, which have been shown to decrease in number with endothelial deletion of Rbpj (Chapman, 2018). Previous studies have shown that Bergmann glia rely on local granular neurons for proper differentiation during development and neurons rely on blood vessels and astrocyte projections as scaffolding for cell migration (Araujo et al., 2019; Xi et al., 2015; Yamada and Watanabe, 2002). It is likely that the endothelial deletion of *Rbpj* could affect one or more of the steps of cerebellar development. The abnormal morphology of astrocytes in the Rbpj mutant cerebellum may be due to a perturbation in the development process. It would be useful to gather similar data at an earlier timepoint to assess any differences in the cerebellar development process.

The relationship between the significantly increased number of cells positive for EdU and GFAP and the lack of significance in the increase in astrocyte area in the Rbpj mutants should also be considered. Increased proliferation might suggest increased number of astrocytes, so the two results are somewhat contradictory to each other. There are visible differences in the morphology of astrocytes of the Rbpj mutant (Figure 19). Again, the cortex is a region with higher instances of abnormal arteriovenous connections in the Rbpj model of AVM. There was a range of results for the cortex, which may suggest a range in phenotypic severity as mentioned before. An increased sample size would reveal trends in GFAP-positive area in the cortex. Also, the morphology of astrocytes is difficult to visualize in the control cortex with GFAP staining (Figure 19 A-B). It may be beneficial to incorporate an additional astrocyte antibody for imaging

purposes. It may also be useful to implement new morphological analyses to accommodate for the diverse morphology of astrocytes in the cortex.

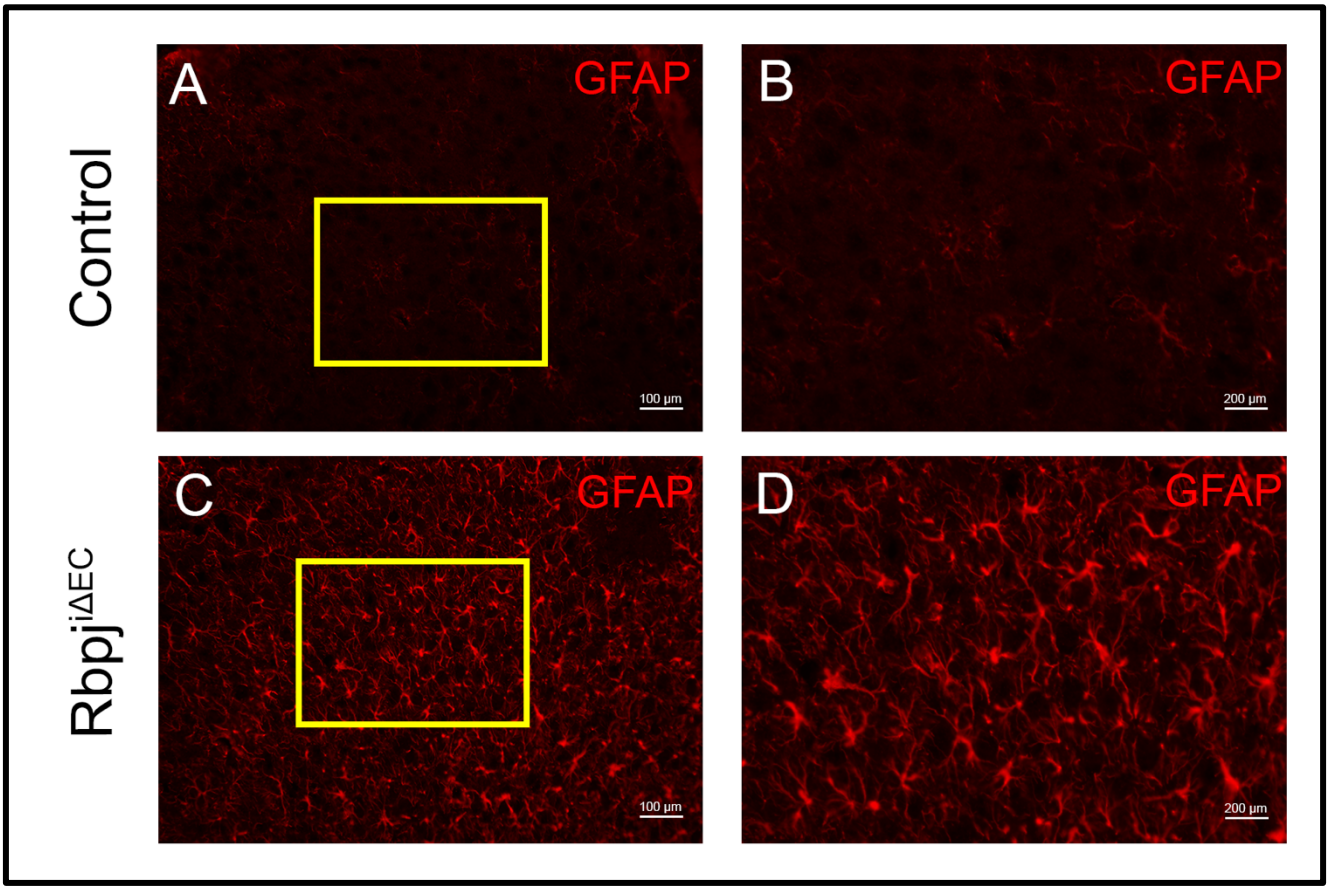

Figure 19. Control and mutant astrocytes in the cortex. Microscope images of GFAP-stained sagittal sections taken in the control (a-b) and Rbpj mutant (d-e) cortex. (a,d) images. (b,e) Images digitally zoomed to show detail.

One of the primary hallmarks of reactive astrocytes is increased expression of the GFAP protein. Despite many attempts at a Western blot analysis, I was unable to produce results to analyze and report. This is most-likely due to nonideal experimental parameters. When conducted at optimal conditions and, likely, a high sample number to account for variability in mutant phenotype, there is promise for this method to yield important information for the study of astrocyte response to endothelial deletion of *Rbpj*. Because of the success of the astrocyte

enrichment, it may be beneficial to use protein from isolated astrocytes, to complete the quantitative Western blotting experiments and analysis.

In order to conduct the qPCR analysis, I first had to isolate astrocytes from the whole brains of my experimental mice. I did so by creating a single cell suspension and separating cells through MACS, but there was variability in isolation yield between experimental samples. The enrichment analysis revealed that there was some contamination by microglia and oligodendrocytes (data not shown), but the sample showed limited contamination by neurons. The results for astrocyte enrichment, presented in Figure 17 of this thesis, represent the first-time astrocyte isolation was attempted in our lab. The success of these first isolations, with no time suggests adjusting parameters and troubleshooting, will allow future experiments, using RNA and proteins from the enriched astrocyte populations.

Though there was a great deal of variability in the qPCR results, there is also promise for this method to reveal valuable insight into how endothelial deletion of *Rbpj* affects astrocytes. The variability in this result could be attributed to multiple factors. The inconclusive qPCR data may be a result of inconsistent experimental conditions, for example three brains were harvested and used for one sample, while one brain was used for another sample. Because of time limitations and mouse availability, we moved forward with qPCR, despite such inconsistencies. The parameters will be adjusted moving forward. The variability may also have been due to the variation in phenotypic severity. This experiment will require replication with increased sample size and improved experimental parameters to yield reliable results. Due to time and tissue constraints, I was also not able to run qPCR analysis on every transcript that I planned to assess.

To optimize astrocyte cell isolations and qPCR, sample size needs to be increased, and experimental conditions need to be developed specifically for astrocytes.

The heterogeneity of astrocytes throughout the brain allows them to serve unique functions based on the needs of the tissue surrounding them. The diversity of astrocyte function leads to the diversity of astrocyte reactivity. In Escartin et al., 2021, where proper definitions and guidelines were established for the study of reactive astrocytes, authors asserted that the binary, A1/A2 astrocyte labels were too general to encompass the complexity of astrocyte function and reaction. One of the initial goals of this thesis was to determine whether reactive astrocytes in the Rbpj AVM model brain are "A1" or "A2," based on the levels of several transcripts that had previously been used to determine the identity of reactive astrocytes (Liddelow et al., 2017). With the publication by Escartin et al. in February 2021, in the middle of development of this thesis, came a reimagined approach to assessing the identity of astrocytes. Instead of specific markers to fit a binary label, the authors recommended an approach shifted to analyses of altered astrocyte functions (Escartin et al., 2021). Regardless, astrocyte reactivity must first be established before astrocytes' impact on surrounding tissue can be investigated.

In this thesis, the approach I took to study astrocytes was to investigate if they became reactive to the "injury" that is the model of AVM. It is important to acknowledge that there is complex communication taking place between cells within the neurovascular unit and it is difficult to point to exactly what is a cause and what is an effect. Astrocytes may react to abnormal vessel connections in the brain, but they may also react to the change in intercellular signaling that takes place, following the endothelial deletion of *Rbpj.* Astrocytes also do not react completely on their own. Previous studies have shown that microglia may play an important role

in astrocyte reactivity (Liddelow et al., 2017; Shinozaki et al., 2017; Streit et al., 1999). This was known more broadly as “gliosis”, but the term may now be outdated because of the establishment of “reactive astrogliosis” as a more accepted term. In previous papers, several of the transcripts that were supposedly indicative of A1 or A2 astrocyte identity were pro and anti-inflammatory markers (Clarke et al., 2018; Das et al., 2020; Liddelow et al., 2017). Inflammation may be an important factor in astrocyte reactivity and microglia would be a good target for further investigation.

FUTURE DIRECTIONS

For future investigation into astrocyte reactivity in response to endothelial deletion of *Rbpj,* I recommend the following:

1. Increasing the sample size for analysis of GFAP-positive area in different brain regions to account for variability in AVM phenotype severity.
2. Expanding EdU proliferation analysis in cerebellum using astrocyte cell body/nuclear marker and neural marker to aid in identification of Bergman glia and Purkinje cells.
3. Expanding hypertrophy analysis to more brain regions.
4. Expanding image analyses to include an alternate antibody for astrocytes and supplemental morphology analyses.
5. Conducting a Western blot experiment to measure GFAP protein expression in control and Rbpj mutant.
6. Optimizing astrocyte isolation protocol to improve purity.
7. Increasing sample size for qPCR, optimizing experimental parameters, and running the full cohort of transcript primers. This would increase the quality of the results and increase statistical power.
8. Using reactive astrocyte markers beyond GFAP. In Escartin et al., 2021, authors stated that GFAP was a strong indicator, but not an absolute marker for reactive astrocytes. This paper includes a list of potential additional markers, such as vimentin and S100 β.
9. Implementing functional analyses, possibly including some in Escartin et al., 2021
10. Investigating the relationship between astrocyte reactivity and microglia activation/infiltration in mutant brain.

CONCLUSION

This thesis is a novel study of astrocyte reactivity in brain AVM. To my knowledge, this will be one of the first comprehensive studies to determine whether and how astrocytes are affected during brain AVM pathogenesis, and it will be the first study on astrocytes in Notch/Rbpj-mediated brain AVM. My data showed evidence for two characteristic signs of reactive astrocytes: hypertrophy and proliferation. Qualitatively, GFAP-positive area appeared increased in mutant brain, though more experiments are necessary for quantitative results. Taken together, my data suggest that astrocytes likely become reactive, following endothelial deletion of Rbpj, and in the context of Rbpj mediated brain AVM. I believe increased sample sizes will increase the statistical power and bring conclusive results to the qPCR analysis, allowing us to describe the molecular signature of these likely-reactive astrocytes. There is room within the experiments from this thesis for technical and statistical improvement, and there is potential for new, reimagined approaches to assessing astrocyte reactivity and the consequences it may have on surrounding brain tissue. This field has great potential and should be investigated further.

With increasing knowledge on the interactivity and communication between cellular members of the neurovascular unit, it is reasonable to assume that a lesion in one cell type may influence the others. My thesis data suggest there may be consequences to astrocytes in response to endothelial deletion of Rbpj. It is clinically relevant to understand if and how astrocytes can affect AVM pathology, because astrocytes play such a major role in the nervous system, and they have the potential to modify the severity of damage incurred to the brain, by AVM. This thesis provides a foundation for future work to determine whether astrocytes play active roles during Rbpj-mediated brain AVM.

ACKNOWLEDGEMENTS

I am very grateful to the following funding sources that allowed me to complete this thesis: Ohio University Biological Sciences Department, Ohio University College of Arts and Sciences, Honors Tutorial College (HTC), and the HTC Apprenticeship.

I would like to thank Dr. Corinne Nielsen. I greatly appreciate her guidance through the process of completing this thesis. She has helped me develop my skills in the lab as a researcher, and outside of the lab as a critical thinker. She has led me with her expertise in the field of AVM while encouraging me to learn and think independently. The fact that she was willing and able to take on not one, but two HTC seniors for their theses, even while adapting to a global pandemic, shows a contagious passion for her research and excellence as a mentor. I would also like to thank graduate students Subhodip Adhicary and Sera Nakisli. Their mentorship and feedback has been invaluable to me and my thesis. The supportive and collaborative environment within Nielsen lab is very conducive to the success of each of its members. I am grateful for my fellow lab members Shruthi Kandalai, Julia LaComb, Alexis LeDantec-Boswell, Kayleigh Fanelli, and Kristen Schuch. I would also like to thank Timothy Wohl, a former member of Nielsen lab, who did the original GFAP imaging work that inspired this thesis.

I would like to thank the Honors Tutorial College for giving me the opportunity to complete this thesis. Specifically, I am grateful for my dean Dr. Donal Skinner, Beth Novak, Breanne Sisler, Kathy White, and Margie Huber. The support I have received from the HTC staff has helped me immensely throughout my time as an undergraduate, especially in the last year in response to COVID-19. I have thoroughly enjoyed my time in HTC and I feel uniquely prepared for my future in science because of the education I have received. I have built friendships and

relationships through HTC that I will treasure for life. My HTC Neuroscience advisor, Dr. Janet Duerr, has been an amazing support over these years. I am so grateful for her and everything she has done for me.

I am especially thankful for my family and friends. They celebrate with me through my successes and are there to encourage me through my hardships. I would not have been able to do any of this without their support.

WORKS CITED

Abla, A. A., Nelson, J., Kim, H., Hess, C. P., Tihan, T. and Lawton, M. T. (2015). Silent arteriovenous malformation hemorrhage and the recognition of "unruptured" arteriovenous malformation patients who benefit from surgical intervention. *Neurosurgery* **76**, 592–600.

Ajiboye, N., Chalouhi, N., Starke, R. M., Zanaty, M. and Bell, R. (2014). Cerebral arteriovenous malformations: evaluation and management. *Sci. World J.* **2014**, 649036.

Araujo, A. P. B., Carpi-Santos, R. and Gomes, F. C. A. (2019). The Role of Astrocytes in the Development of the Cerebellum. *Cerebellum Lond. Engl.* **18**, 1017–1035.

Bardehle, S., Krüger, M., Buggenthin, F., Schwausch, J., Ninkovic, J., Clevers, H., Snippert, H. J., Theis, F. J., Meyer-Luehmann, M., Bechmann, I., et al. (2013). Live imaging of astrocyte responses to acute injury reveals selective juxtavascular proliferation. *Nat. Neurosci.* **16**, 580–586.

Becerra-Calixto, A. and Cardona-Gómez, G. P. (2017). The role of astrocytes in neuroprotection after brain stroke: potential in cell therapy. *Front. Mol. Neurosci.* **10**, 88.

Bell, A. H., Miller, S. L., Castillo-Melendez, M. and Malhotra, A. (2020). The neurovascular unit: effects of brain insults during the perinatal period. *Front. Neurosci.* **13**, 1452.

Brain AVM (arteriovenous malformation) - Diagnosis and treatment - Mayo Clinic.

Brain AVM (arteriovenous malformation) - Symptoms and causes *Mayo Clin.*

Chapman, A. D. (2018). A novel role for endothelial Rbpj in postnatal cerebellum morphogenesis.

Choudhury, G. R. and Ding, S. (2016). Reactive astrocytes and therapeutic potential in focal ischemic stroke. *Neurobiol. Dis.* **85**, 234–244.

Clarke, L. E., Liddelow, S. A., Chakraborty, C., Münch, A. E., Heiman, M. and Barres, B. A. (2018). Normal aging induces A1-like astrocyte reactivity. *Proc. Natl. Acad. Sci.* **115**, E1896–E1905.

Das, S., Li, Z., Noori, A., Hyman, B. T. and Serrano-Pozo, A. (2020). Meta-analysis of mouse transcriptomic studies supports a context-dependent astrocyte reaction in acute CNS injury versus neurodegeneration. *J. Neuroinflammation* **17**, 227.

Escartin, C., Galea, E., Lakatos, A., O'Callaghan, J. P., Petzold, G. C., Serrano-Pozo, A., Steinhäuser, C., Volterra, A., Carmignoto, G., Agarwal, A., et al. (2021). Reactive Astrocyte Nomenclature, Definitions, and Future Directions. *Nat. Neurosci.* **24**, 312–325.

Friedlander, R. M. (2007). Arteriovenous malformations of the brain. *N. Engl. J. Med.* **356**, 2704–2712.

Gridley, T. (2010). Notch Signaling in the Vasculature. *Curr. Top. Dev. Biol.* **92**, 277–309.

Guttmacher, A. E., Marchuk, D. A. and White, R. I. (1995). Hereditary Hemorrhagic Telangiectasia. *N. Engl. J. Med.* **333**, 918–924.

Hawkins, B. T. and Davis, T. P. (2005). The blood-brain barrier/neurovascular unit in health and disease. *Pharmacol. Rev.* **57**, 173–185.

Imura, T., Tane, K., Toyoda, N. and Fushiki, S. (2008). Endothelial cell-derived bone morphogenetic proteins regulate glial differentiation of cortical progenitors. *Eur. J. Neurosci.* **27**, 1596–1606.

Kim, Y., Park, J. and Choi, Y. K. (2019). The role of astrocytes in the central nervous system focused on BK channel and heme oxygenase metabolites: a review. *Antioxidants* **8**,.

Koehler, R. C., Gebremedhin, D. and Harder, D. R. (2006). Role of astrocytes in cerebrovascular regulation. *J. Appl. Physiol.* **100**, 307–317.

Krebs, L. T., Shutter, J. R., Tanigaki, K., Honjo, T., Stark, K. L. and Gridley, T. (2004). Haploinsufficient lethality and formation of arteriovenous malformations in Notch pathway mutants. *Genes Dev.* **18**, 2469–2473.

Lawson, N. D., Scheer, N., Pham, V. N., Kim, C.-H., Chitnis, A. B., Campos-Ortega, J. A. and Weinstein, B. M. (2001). Notch signaling is required for arterial-venous differentiation during embryonic vascular development. *Development* **128**, 3675–3683.

Lee, M. L., Martinez-Lozada, Z., Krizman, E. N. and Robinson, M. B. (2017). Brain endothelial cells induce astrocytic expression of the glutamate transporter GLT-1 by a Notch-dependent mechanism. *J. Neurochem.* **143**, 489–506.

Li, P., Zhang, L., Chen, D., Zeng, M. and Chen, F. (2018). Focal neurons: another source of vascular endothelial growth factor in brain arteriovenous malformation tissues? *Neurol. Res.* **40**, 122–129.

Liddelow, S. A. and Barres, B. A. (2017). Reactive astrocytes: production, function, and therapeutic potential. *Immunity* **46**, 957–967.

Liddelow, S. A., Guttenplan, K. A., Clarke, L. E., Bennett, F. C., Bohlen, C. J., Schirmer, L., Bennett, M. L., Münch, A. E., Chung, W.-S., Peterson, T. C., et al. (2017). Neurotoxic reactive astrocytes are induced by activated microglia. *Nature* **541**, 481–487.

Ma, S., Kwon, H. J. and Huang, Z. (2012). A functional requirement for astroglia in promoting blood vessel development in the early postnatal brain. *PLoS ONE* **7**, e48001.

Mast Henning, Mohr J. P., Osipov Andrei, Pile-Spellman John, Marshall Randolph S., Lazar Ronald M., Stein Bennett M., and Young William L. (1995). 'Steal' is an unestablished mechanism for the clinical presentation of cerebral arteriovenous malformations. *Stroke* **26**, 1215–1220.

Mohr, J. P. (2015). *A Randomized Trial of Unruptured Brain Arteriovenous Malformations*. clinicaltrials.gov.

Mohr, J. P., Parides, M. K., Stapf, C., Moquete, E., Moy, C. S., Overbey, J. R., Salman, R. A.-S., Vicaut, E., Young, W. L., Houdart, E., et al. (2014). Medical management with or without interventional therapy for unruptured brain arteriovenous malformations (ARUBA): a multicentre, non-blinded, randomised trial. *Lancet* **383**, 614–621.

Murphy, P. A., Lam, M. T. Y., Wu, X., Kim, T. N., Vartanian, S. M., Bollen, A. W., Carlson, T. R. and Wang, R. A. (2008). Endothelial Notch4 signaling induces hallmarks of brain arteriovenous malformations in mice. *Proc. Natl. Acad. Sci. U. S. A.* **105**, 10901–10906.

Muzumdar, M. D., Tasic, B., Miyamichi, K., Li, L. and Luo, L. (2007). A global double-fluorescent Cre reporter mouse. *Genes. N. Y. N 2000* **45**, 593–605.

Nelson, A. R., Sweeney, M. D., Sagare, A. P. and Zlokovic, B. V. (2016). Neurovascular dysfunction and neurodegeneration in dementia and Alzheimer's disease. *Biochim. Biophys. Acta* **1862**, 887–900.

Nielsen, C. M., Cuervo, H., Ding, V. W., Kong, Y., Huang, E. J. and Wang, R. A. (2014). Deletion of Rbpj from postnatal endothelium leads to abnormal arteriovenous shunting in mice. *Development* **141**, 3782–3792.

Oberheim, N. A., Goldman, S. A. and Nedergaard, M. (2012). Heterogeneity of astrocytic form and function. *Methods Mol. Biol. Clifton NJ* **814**, 23–45.

Park, S. O., Wankhede, M., Lee, Y. J., Choi, E.-J., Fliess, N., Choe, S.-W., Oh, S.-H., Walter, G., Raizada, M. K., Sorg, B. S., et al. (2009). Real-time imaging of de novo arteriovenous malformation in a mouse model of hereditary hemorrhagic telangiectasia. *J. Clin. Invest.* **119**, 3487–3496.

Sato, Y., Uchida, Y., Hu, J., Young-Pearse, T. L., Niikura, T. and Mukouyama, Y.-S. (2017). Soluble APP functions as a vascular niche signal that controls adult neural stem cell number. *Dev. Camb. Engl.* **144**, 2730–2736.

Selhorst, S. A. (2019). Endothelial deletion of Rbpj leads to perivascular abnormalities in the brain.

Sheth, R. D. and Bodensteiner, J. B. (1995). Progressive neurologic impairment from an arteriovenous malformation vascular steal. *Pediatr. Neurol.* **13**, 352–354.

Shimada, I. S., Borders, A., Aronshtam, A. and Spees, J. L. (2011). Proliferating reactive astrocytes are regulated by Notch-1 in the peri-infarct area after stroke. *Stroke* **42**, 3231–3237.

Shinozaki, Y., Shibata, K., Yoshida, K., Shigetomi, E., Gachet, C., Ikenaka, K., Tanaka, K. F. and Koizumi, S. (2017). Transformation of astrocytes to a neuroprotective phenotype by microglia via P2Y1 receptor downregulation. *Cell Rep.* **19**, 1151–1164.

Sörensen, I., Adams, R. H. and Gossler, A. (2009). DLL1-mediated Notch activation regulates endothelial identity in mouse fetal arteries. *Blood* **113**, 5680–5688.

Spetzler, R. F. and Martin, N. A. (1986). A proposed grading system for arteriovenous malformations. *J. Neurosurg.* **65**, 476–483.

Stapf, C., Mast, H., Sciacca, R. R., Choi, J. H., Khaw, A. V., Connolly, E. S., Pile-Spellman, J. and Mohr, J. P. (2006). Predictors of hemorrhage in patients with untreated brain arteriovenous malformation. *Neurology* **66**, 1350–1355.

Stevens, B. and Muthukumar, A. K. (2016). Differences among astrocytes. *Science* **351**, 813–813.

Streit, W. J., Walter, S. A. and Pennell, N. A. (1999). Reactive microgliosis. *Prog. Neurobiol.* **57**, 563–581.

Tabata, H. (2015). Diverse subtypes of astrocytes and their development during corticogenesis. *Front. Neurosci.* **9**, 114.

Tanigaki, K., Han, H., Yamamoto, N., Tashiro, K., Ikegawa, M., Kuroda, K., Suzuki, A., Nakano, T. and Honjo, T. (2002). Notch-RBP-J signaling is involved in cell fate determination of marginal zone B cells. *Nat. Immunol.* **3**, 443.

Teo, M., St. George, J. and Lawton, M. T. (2015). Time for BARBADOS after ARUBA trial. *Br. J. Neurosurg.* **29**, 635–636.

Tu, J., Stoodley, M. A., Morgan, M. K. and Storer, K. P. (2006). Ultrastructure of perinidal capillaries in cerebral arteriovenous malformations. *Neurosurgery* **58**, 961–970.

Udan, R. S., Culver, J. C. and Dickinson, M. E. (2013). Understanding vascular development. *Wiley Interdiscip. Rev. Dev. Biol.* **2**, 327–346.

Wei, Y., Gong, J., Xu, Z., Thimmulappa, R. K., Mitchell, K. L., Welsbie, D. S., Biswal, S. and Duh, E. J. (2015). Nrf2 in ischemic neurons promotes retinal vascular regeneration through regulation of semaphorin 6A. *Proc. Natl. Acad. Sci.* **112**, E6927–E6936.

Winkler, E. A., Birk, H., Burkhardt, J.-K., Chen, X., Yue, J. K., Guo, D., Rutledge, W. C., Lasker, G. F., Partow, C., Tihan, T., et al. (2018). Reductions in brain pericytes are associated with arteriovenous malformation vascular instability. *J. Neurosurg.* **129**, 1464–1474.

Wolburg-Buchholz, K., Mack, A. F., Steiner, E., Pfeiffer, F., Engelhardt, B. and Wolburg, H. (2009). Loss of astrocyte polarity marks blood–brain barrier impairment during experimental autoimmune encephalomyelitis. *Acta Neuropathol. (Berl.)* **118**, 219–233.

Xi, Y., Chen, W. J., Deng, J. X., Cui, Z. J., Liu, H. L., Yan, M. C., Deng, J. B. and Wu, P. (2015). Vasculature-guided neural migration in mouse cerebellum. *Ital. J. Zool.* **82**, 15–24.

Yamada, K. and Watanabe, M. (2002). Cytodifferentiation of Bergmann glia and its relationship with Purkinje cells. *Anat. Sci. Int.* **77**, 94–108.

Yamamizu, K., Matsunaga, T., Uosaki, H., Fukushima, H., Katayama, S., Hiraoka-Kanie, M., Mitani, K. and Yamashita, J. K. (2010). Convergence of Notch and β-catenin signaling induces arterial fate in vascular progenitors. *J. Cell Biol.* **189**, 325–338.

Yun, S. P., Kam, T.-I., Panicker, N., Kim, S., Oh, Y., Park, J.-S., Kwon, S.-H., Park, Y. J., Karuppagounder, S. S., Park, H., et al. (2018). Block of A1 astrocyte conversion by microglia is neuroprotective in models of Parkinson's disease. *Nat. Med.* **24**, 931–938.

Zerlin, M. and Goldman, J. E. (1997). Interactions between glial progenitors and blood vessels during early postnatal corticogenesis: Blood vessel contact represents an early stage of astrocyte differentiation. *J. Comp. Neurol.* **387**, 537–546.

ZhuGe, Q., Zhong, M., Zheng, W., Yang, G.-Y., Mao, X., Xie, L., Chen, G., Chen, Y., Lawton, M. T., Young, W. L., et al. (2009). Notch-1 signalling is activated in brain arteriovenous malformations in humans. *Brain* **132**, 3231–3241.